J. Fluid Mech. (1997), *vol.* 342, *pp.* 231–261. Printed in the United Kingdom

Direct numerical simulations of the turbulence evolution in a uniformly sheared and stably stratified flow

By FRANK G. JACOBITZ, SUTANU SARKAR AND CHARLES W. VAN ATTA†

Department of Applied Mechanics and Engineering Sciences, University of California, San Diego, La Jolla, CA 92093-0411, USA.

(Received 13 December 1995 and in revised form 8 December 1996)

Direct numerical simulations (DNS) are performed to investigate the evolution of turbulence in a uniformly sheared and stably stratified flow. The spatial discretization is accomplished by a spectral collocation method, and the solution is advanced in time with a third-order Runge–Kutta scheme. The turbulence evolution is found to depend strongly on at least three parameters: the gradient Richardson number Ri, the initial value of the Taylor microscale Reynolds number Re_λ, and the initial value of the shear number SK/ϵ. The effect of each parameter is individually studied while the remaining parameters are kept constant. The evolution of the turbulent kinetic energy K is found to follow approximately an exponential law. The shear number SK/ϵ, whose effect has not been investigated in previous studies, was found to have a strong non-monotone influence on the turbulence evolution. Larger values of the shear number do not necessarily lead to a larger value of the eventual growth rate of the turbulent kinetic energy. Variation of the Reynolds number Re_λ indicated that the turbulence growth rate tends to become insensitive to Re_λ at the higher end of the Re_λ range studied here. The dependence of the critical Richardson number Ri_{cr}, which separates asymptotic growth of the turbulent kinetic energy K from asymptotic decay, on the initial values of the Reynolds number Re_λ and the shear number SK/ϵ was also obtained. It was found that the critical Richardson number varied over the range $0.04 < Ri_{cr} < 0.17$ in our DNS due to its strong dependence on Reynolds and shear numbers.

1. Introduction

During the past decade, both numerical simulations and laboratory experiments of homogeneous turbulence in a stably stratified shear flow have been performed to investigate the effects of shear and stratification on the turbulence evolution. These studies were undertaken with the goal of explaining and understanding the turbulent microstructure of geophysical flows in the atmosphere and ocean. The present paper considers stratified shear flow with a uniform gradient of the ambient density S_ρ and uniform mean shear rate S. The primary non-dimensional parameter that determines the turbulence evolution in such a flow is the gradient Richardson number $Ri = N^2/S^2$, the square of the ratio of the Brunt–Väisälä frequency $N =$

† Also Scripps Institution of Oceanography.

$[(-g\mathrm{d}\bar{\rho}/\mathrm{d}z)/\rho_0]^{1/2}$ and the mean shear rate S. A critical value of the Richardson number Ri_{cr} can be found for which the turbulent kinetic energy K stays constant in time, grows in time for $Ri < Ri_{cr}$, and decays in time for $Ri > Ri_{cr}$. Knowledge of the critical Richardson number is therefore important as it divides the asymptotic fate of the nonlinearly evolving turbulence into growth or decay. The significance of the Richardson number was first mentioned in Taylor's 1914 Adams Prize Essay†. Subsequent studies by Richardson (1920), Prandtl (1930), Taylor (1931), Goldstein (1931), and Miles (1986) confirmed the important role of the Richardson number Ri and established $Ri > 1$ as the sufficient condition for stability based on energy arguments. Linear, inviscid stability theory yields $Ri > 1/4$ as the sufficient condition for stability of a stratified shear flow (Miles 1961 and Howard 1961). An analysis of the equations of homogeneous turbulence in a stratified shear flow was applied to atmospheric flow by Batchelor (1953*b*) and Townsend (1957). Using experimental observations of entrainment, Townsend estimated the critical value of the Richardson number to be about $Ri_{cr} = 0.08$.

The first direct numerical simulations (DNS) of homogeneous turbulence in a stratified shear flow were performed by Gerz, Schumann & Elghobashi (1989). In their investigation shear periodic boundary conditions were used in combination with a finite difference/spectral collocation method. The simulations were performed on a grid with 64^3 points. The Richardson number was varied over the range $0 \leqslant Ri \leqslant 1$. Gerz *et al.* found that the evolution of the turbulent kinetic energy K depends strongly on the Richardson number Ri. The initial energy partition η, the ratio of the potential to kinetic energy, was found to lead to different initial transients but not to influence the turbulence evolution over a long period of time. Gerz *et al.* investigated the occurrence of counter-gradient heat fluxes which were more prominent for large Richardson numbers and high molecular Prandtl numbers.

Holt, Koseff & Ferziger (1992) investigated the turbulence evolution in a homogeneous stably stratified shear flow using purely periodic boundary conditions in combination with a spectral collocation method. The simulations were performed on a grid with 128^3 points. The simulations covered a parameter range $0 \leqslant Ri \leqslant 1$ and $20 \leqslant Re_\lambda \leqslant 100$, where Re_λ is the Taylor microscale Reynolds number. They divided the turbulence evolution into shear- or buoyancy-dominated regimes for the Richardson number smaller or larger than the transitional value Ri_t for which the vertical density flux vanishes. Simulations with constant turbulent kinetic energy K were found to lie in the shear-dominated regime, that is $Ri_{cr} < Ri_t$. Holt *et al.* investigated the influence of the initial energy partition η and of the molecular Prandtl number Pr and agreed with the conclusions of Gerz *et al.* (1989). In addition the dependence of the turbulence evolution on the Reynolds number Re_λ was addressed. It was found that the critical Richardson number Ri_{cr} increases with the Reynolds number Re_λ.

Kaltenbach, Gerz & Schumann (1994) performed large-eddy simulations to investigate the turbulent transport in a homogeneous stably stratified shear flow. They observed that vertical overturning and mixing is suppressed when the inverse Froude number $Fi = Nl/q$ (l is an integral length scale of the velocity, and q is the root-mean-square velocity) exceeds a critical value of about 3.

Rohr *et al.* (1988) performed the first successful experiments on homogeneous turbulence in a stably stratified shear flow in a salt-stratified water channel. A

† According to Taylor (1931) and Miles (1961). The Adams Prize Essay is not available to the authors.

variation of the Richardson number Ri led to constant vertical velocity fluctuations u_3^{rms} for $Ri = Ri_{cr} = 0.25 \pm 0.05$, growing u_3^{rms} for $Ri < Ri_{cr}$, and decaying u_3^{rms} for $Ri > Ri_{cr}$.

Piccirillo & Van Atta (1997) investigated the turbulence evolution in a homogeneous stably stratified shear flow using a thermally stratified wind tunnel, in which they varied the Reynolds number Re_λ over a small range by using a variety of different turbulence-generating grids. They found a decrease of the critical Richardson number Ri_{cr} with increasing grid size and thus increasing Reynolds number Re_λ. Holt *et al.* (1992), on the other hand, found an increase of Ri_{cr} with increasing Re_λ.

The evolution of high-shear-number flow has been studied analytically and numerically. For high shear numbers SK/ϵ, the nonlinear term in the momentum equation may become less important than the shear forcing term. Therefore the nonlinear term can be neglected, and a simplified analysis can be performed instead. This approach is known as rapid distortion theory (RDT). An introduction to RDT is given in the review article by Hunt (1978) and more recently by Savill (1987). The application of RDT to viscous unstratified shear flow by Rogers (1991) predicts eventual decay of the turbulent kinetic energy after initial algebraic growth. Because of the neglect of the nonlinear term, RDT results formally apply for short-time evolution ($St = O(1)$). An experimental study of unstratified high-shear-number flow was recently performed by Souza, Nguyen & Tavoularis (1995). They found that the magnitude of the Reynolds shear stress anisotropy decreases at large shear numbers.

A motivation of this study is to explain the apparently different dependence of the critical Richardson number Ri_{cr} on the Reynolds number Re_λ observed in direct numerical simulations by Holt *et al.* (1992) and experimental investigations by Piccirillo & Van Atta (1997). Assuming that both DNS and experiments are correct, we hypothesized that, perhaps, there is another parameter in the problem. An analysis of the governing equations shows that the shear number SK/ϵ is an additional parameter, and an inspection of the data of Piccirillo & Van Atta (1997) shows that the different turbulence-generating grids lead to not only different Reynolds numbers but also different shear numbers. We perform a systematic DNS study of the effect of the shear number SK/ϵ on the turbulence evolution and show that, indeed, the shear number has a strong influence. As this work progressed, the DNS results prompted a timely assessment of the effect of the shear number SK/ϵ in the laboratory experiments, as described in Piccirillo & Van Atta (1997). It should be noted that the previous numerical studies did not investigate the role of SK/ϵ.

An additional motivation of the present study is to perform direct numerical simulations at the higher Reynolds numbers accessible with today's supercomputers, in order to investigate the possibility of a decreased influence of the Reynolds number Re_λ on the turbulence evolution at high values of Re_λ.

In the following section, the evolution and transport equations used in this study are introduced, and the non-dimensional parameters governing the turbulence evolution are derived. In §3 the numerical method is described, and the initial conditions and their importance for effective parameterization are addressed. The dependence of the evolution of the turbulent kinetic energy on the non-dimensional parameters derived in §2 is presented in §4. In §5 the asymptotic evolution of the turbulent kinetic energy is summarized. The dependence of the critical Richardson number on the remaining non-dimensional parameters is discussed in §6. Section 7 summarizes our conclusions on the turbulence evolution in a stably stratified shear flow. The numerical method used in this study is validated in an Appendix.

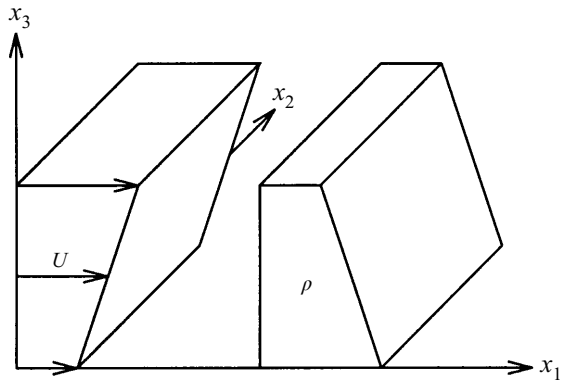

FIGURE 1. Sketch of the mean velocity and the mean density.

2. Mathematical preliminaries

In this section the equations of motion used to describe the evolution of a turbulent stratified shear flow are presented. In addition the transport equations for second-order moments are introduced. Finally the non-dimensional parameters governing the turbulence evolution are derived.

2.1. *Equations of motion*

Our study of a turbulent stratified shear flow is based on the continuity equation of an incompressible fluid, the Navier–Stokes equation and a transport equation for the density. In the following, X_i is the ith coordinate of an orthonormal Cartesian coordinate system, U_i is the ith component of the total velocity, ϱ is the total density, P is the total pressure, g is the gravitational constant, μ is the molecular viscosity of the fluid, and κ is the diffusion coefficient. The dependent variables $U_i = \overline{U}_i + u_i$, $\varrho = \overline{\varrho} + \rho$, and $P = \overline{P} + p$ are decomposed into a mean part (denoted by an overbar) and a fluctuating part (denoted by lower-case or alternative greek letters). The mean velocity $\overline{U}_i = SX_3\delta_{i1}$ and the mean density $\overline{\varrho} = \rho_0 + S_\rho X_3$ are given by the constant velocity gradient $S = \partial\overline{U}_1/\partial X_3$ and the constant density gradient $S_\rho = \partial\overline{\varrho}/\partial X_3$, as shown in figure 1. It is assumed that a mean pressure gradient balances the mean buoyancy force, that is $0 = -\partial\overline{P}/\partial X_3 - g(\rho_0 + S_\rho X_3)$. This decomposition is introduced into the equations of motion. Furthermore the Boussinesq approximation is employed.

Spectral accuracy in the spatial discretization can be obtained by the use of periodic boundary conditions, but due to the effect of shear, periodic boundary conditions cannot be applied directly to the equations of motion. In previous simulations, Gerz *et al.* (1989) used shear periodic boundary conditions in combination with finite difference approximations. To use strictly periodic boundary conditions, the equations must be transformed into a frame of reference that is moving with the mean flow. This approach was originally developed by Rogallo (1981), and it has been used in a number of simulations of turbulent shear flow (Rogers, Moin & Reynolds 1986), compressible turbulent shear flow (Sarkar 1995) and turbulent stratified shear flow (Holt *et al.* 1992). After non-dimensionalization, the transformation $t = T$ and $x_i = X_i - STX_3\delta_{i1}$ yields the following equations:

$$\frac{\partial u_j}{\partial x_j} - St\frac{\partial u_3}{\partial x_1} = 0, \tag{2.1}$$

$$\frac{\partial u_i}{\partial t}+u_j\frac{\partial u_i}{\partial x_j}-Stu_3\frac{\partial u_i}{\partial x_1}+Su_3\delta_{i1}=-\frac{1}{\rho_0}\left(\frac{\partial p}{\partial x_i}-St\frac{\partial p}{\partial x_1}\delta_{i3}\right)-G\rho\delta_{i3}$$
$$+\frac{1}{Re}\left(\frac{\partial^2 u_i}{\partial x_j\partial x_j}-2St\frac{\partial^2 u_i}{\partial x_1\partial x_3}+S^2t^2\frac{\partial^2 u_i}{\partial x_1\partial x_1}\right), \tag{2.2}$$

$$\frac{\partial \rho}{\partial t}+u_j\frac{\partial \rho}{\partial x_j}-Stu_3\frac{\partial \rho}{\partial x_1}+S_\rho u_3=\frac{1}{RePr}\left(\frac{\partial^2 \rho}{\partial x_j\partial x_j}-2St\frac{\partial^2 \rho}{\partial x_1\partial x_3}+S^2t^2\frac{\partial^2 \rho}{\partial x_1\partial x_1}\right) \tag{2.3}$$

Here $Re = UL/\nu$ is the Reynolds number, $Pr = \nu/\kappa$ is the Prandtl number, and $G = gL/U^2$ is the non-dimensional gravity coefficient. U, L, and ρ_0 are characteristic scales for velocity, length, and density, respectively. The numerical method used to solve this set of equations is introduced in §3.1.

2.2. *Transport equations*

In this subsection the transport equations for second-order moments are derived. The overbar $\overline{a}$ denotes the volume average of a, which is the appropriate Reynolds average in the case of homogeneous flow studied here. The homogeneity is preserved due to the uniformity of the ambient density gradient S_ρ and the mean shear rate S as discussed by Batchelor (1953*a*). The transport equation for the Reynolds stress $R_{ij} = \overline{u_iu_j}$ is derived from the ith and jth components of the momentum equation:

$$\frac{\mathrm{d}}{\mathrm{d}t}R_{ij} = P_{ij} - B_{ij} + T_{ij} - \epsilon_{ij}, \tag{2.4}$$

$$P_{ij} = -S(\overline{u_iu_3}\delta_{j1} + \overline{u_ju_3}\delta_{i1}), \tag{2.5}$$

$$B_{ij} = \frac{g}{\rho_0}(\overline{u_i\rho}\delta_{j3} + \overline{u_j\rho}\delta_{i3}), \tag{2.6}$$

$$T_{ij} = \frac{1}{\rho_0}\left(\overline{p\frac{\partial u_i}{\partial x_j}} + \overline{p\frac{\partial u_j}{\partial x_i}}\right), \tag{2.7}$$

$$\epsilon_{ij} = 2\nu\overline{\frac{\partial u_i}{\partial x_k}\frac{\partial u_j}{\partial x_k}}. \tag{2.8}$$

Here P_{ij} is the production term, B_{ij} the buoyancy term, T_{ij} the pressure-strain term, and ϵ_{ij} the dissipation term. The trace of this equation gives the transport equation for the kinetic energy $K = \overline{u_iu_i}/2$:

$$\frac{\mathrm{d}}{\mathrm{d}t}K = \frac{\mathrm{d}}{\mathrm{d}t}\left(\tfrac{1}{2}\overline{u_iu_i}\right) = P - B - \epsilon, \tag{2.9}$$

$$P = -S\overline{u_1u_3}, \tag{2.10}$$

$$B = \frac{g}{\rho_0}\overline{u_3\rho}, \tag{2.11}$$

$$\epsilon = \nu\overline{\frac{\partial u_i}{\partial x_k}\frac{\partial u_i}{\partial x_k}}. \tag{2.12}$$

In addition, the anisotropy tensor b_{ij} is defined as

$$b_{ij} = \frac{\overline{u_iu_j}}{\overline{u_ku_k}} - \tfrac{1}{3}\delta_{ij}. \tag{2.13}$$

The transport equations for the mass fluxes $M_i = \overline{u_i\rho}$ are derived from the momentum equation and the transport equation for the density:

$$\frac{\mathrm{d}}{\mathrm{d}t}M_i = -S\overline{u_i\rho} - S_\rho\overline{u_iu_3} - \frac{g}{\rho_0}\overline{\rho\rho}\delta_{i3} + \frac{1}{\rho_0}\overline{p\frac{\partial\rho}{\partial x_i}} - \frac{\nu}{\kappa}(\nu+\kappa)\overline{\frac{\partial u_i}{\partial x_k}\frac{\partial\rho}{\partial x_k}}. \tag{2.14}$$

Finally the transport equation for the density variance $\overline{\rho\rho}$ is derived from the transport equation:

$$\frac{\mathrm{d}}{\mathrm{d}t}\left(\tfrac{1}{2}\overline{\rho\rho}\right) = P_\rho - \chi, \tag{2.15}$$

$$P_\rho = -S_\rho\overline{u_3\rho}, \tag{2.16}$$

$$\chi = \kappa\overline{\frac{\partial\rho}{\partial x_k}\frac{\partial\rho}{\partial x_k}}. \tag{2.17}$$

The potential energy K_ρ can be computed from the density variance:

$$K_\rho = \frac{1}{2}\frac{g}{\rho_0|S_\rho|}\overline{\rho\rho}. \tag{2.18}$$

2.3. *Parameters governing the turbulence evolution*

To derive the non-dimensional parameters governing the turbulence evolution, the transport equation for the turbulent kinetic energy K is scaled. Let q be the characteristic velocity scale, l the characteristic length scale and r the characteristic density scale. A characteristic time scale for the turbulence evolution is then given by $\tau = l/q$. In addition the Taylor microscale λ is introduced as a derivative length scale by $\epsilon = 5\nu q^2/\lambda^2$. The terms of the transport equation for the kinetic energy K are divided by the dissipation ϵ:

$$\underbrace{\frac{1}{\epsilon}\frac{\mathrm{d}}{\mathrm{d}t}K}_{1} = \underbrace{\frac{P}{\epsilon}}_{2} - \underbrace{\frac{B}{\epsilon}}_{3} - 1 \tag{2.19}$$

and scaled as follows:

$$O(\text{term } 1) = Re_\lambda\lambda/l, \tag{2.20}$$

$$O(\text{term } 2) = SK/\epsilon, \tag{2.21}$$

$$O(\text{term } 3) = Ri\frac{L_e}{l}\left(\frac{SK}{\epsilon}\right)^2\frac{1}{Re_\lambda}\frac{l}{\lambda}. \tag{2.22}$$

Here $Re_\lambda = q\lambda/\nu$ denotes the Reynolds number based on the Taylor microscale, $Ri = -(gS_\rho)/(\rho_0S^2)$ the Richardson number, and $L_e = r/S_\rho$ the Ellison scale. The kinetic energy is $K = O(q^2)$. Therefore, the non-dimensional parameters governing the turbulence evolution for this low-Reynolds-number scaling are the Richardson number Ri, the Taylor microscale Reynolds number Re_λ and the shear number SK/ϵ. In addition, the initial conditions influence the turbulence evolution by the length-scale ratios λ/l of the velocity fields and L_e/l of the density field.

For high Reynolds numbers, the dissipation varies as $\epsilon = O(q^3/l)$ or equivalently $O(l/\lambda) = Re_\lambda$. This simplifies the scaling to

$$O(\text{term } 1) = 1, \tag{2.23}$$

$$O(\text{term } 2) = SK/\epsilon, \tag{2.24}$$

$$O(\text{term } 3) = Ri\frac{L_e}{l}\left(\frac{SK}{\epsilon}\right)^2. \tag{2.25}$$

Therefore, the non-dimensional parameters governing the turbulence evolution for the high-Reynolds-number scaling are the Richardson number Ri, the shear number SK/ϵ, and the ratio L_e/l.

Additional parameters can be obtained from the evolution equation of the potential energy. These parameters are not considered in this investigation. Effects of a variation of the molecular Prandtl number Pr and the initial energy partition η, the ratio of potential to kinetic energy, were considered by Gerz *et al.* (1989) and Holt *et al.* (1992). The effect of varying the shear number SK/ϵ was not studied in previous investigations.

We emphasize that, for a given initial spectral shape of the flow perturbations, a parameterization based on the initial values of the Reynolds number Re_λ and the shear number SK/ϵ is possible, because initially different values of these parameters remain different throughout all simulations performed in this study, as shown in figures 17(*a*) and 17(*b*).

3. Numerical procedure

In this section the numerical method is described, and the initial conditions and their importance are discussed. A validation of the numerical method is given in the Appendix.

3.1. *Numerical algorithm*

The numerical scheme uses a spectral collocation method for the spatial discretization. To compute spatial partial derivatives, the dependent variables are transformed into Fourier space using the fast Fourier transformation algorithm, multiplied with the corresponding wavenumbers, and transformed back into physical space. Second derivatives are computed by applying this method successively. The nonlinear terms are computed in physical space.

The solution is advanced in time using a third-order Runge–Kutta method. During the time advancement the coordinate system in the moving frame of reference becomes more and more skewed. Following a method originally devised by Rogallo (1981), the coordinate system is reoriented from $+45^\circ$ to -45° using the periodic structure of the dependent variables. The regridding procedure produces aliasing errors. These errors are controlled by truncation of the affected modes ($2k_{max}/3 < k < k_{max}$) before and after the regridding procedure.

The results presented here are from simulations using 128^3 grid points, with the following exceptions. The low-Reynolds-number $Re_\lambda \leqslant 22.36$ and low-shear-number $SK/\epsilon \leqslant 4.0$ simulations are performed on a 96^3 grid, and the high-Reynolds-number simulations $Re_\lambda \geqslant 67.08$ are performed on a 144^3 grid.

3.2. *Initial conditions*

The initial spectra have to be defined carefully to allow a parameterization of the flow evolution based on the initial values of the parameters discussed in §2.3. Usually a random number generator is used to produce the initial fluctuating fields. These fields follow a specified initial energy spectrum and fulfil the continuity equation, but they contain no phase information and have no initial spectral transfer. The energy spectrum E is half the shell average of the squared amplitude of the three-dimensional Fourier transformation of the velocity. Initial energy spectra used in

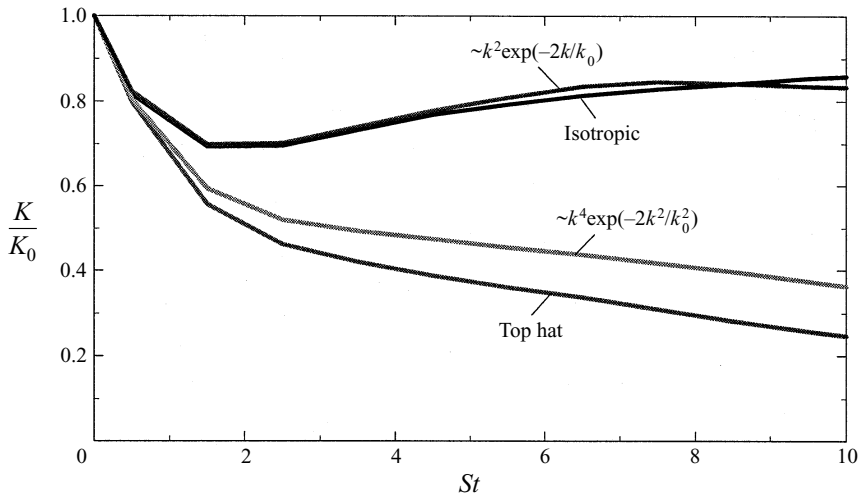

FIGURE 2. Evolution of the turbulent kinetic energy K for different initial spectra. The initial values of the non-dimensional parameters for all cases are $Ri = 0.08$, $Re_\lambda = 22.36$, and $SK/\epsilon = 2.0$.

previous investigations include the top-hat spectrum (Holt *et al.* 1992)

$$E(k) = \begin{cases} E_0 & \text{for } k_1 < k < k_2 \\ 0 & \text{elsewhere,} \end{cases} \tag{3.1}$$

and the exponential spectrum (Sarkar 1995)

$$E(k) = E_0 k^4 \exp(-2k^2/k_0^2). \tag{3.2}$$

Unfortunately these spectra result in an initial transient in the simulations that does not allow a parameterization based on initial values. In figure 2 the evolution of the turbulent kinetic energy K is shown for simulations with different initial radial spectra but identical initial values of the Richardson number $Ri = 0.08$, the Reynolds number $Re_\lambda = 22.36$, and the shear number $SK/\epsilon = 2.0$. The simulations with equations (3.1) and (3.2) as initial spectra show a large initial decay of K during the transient phase and finally continue to decay. In figures 3(*a*) and 3(*b*) the evolution of the Reynolds number Re_λ and the shear number SK/ϵ are shown. During the initial transient these numbers exhibit a large drop. Therefore their initial values are not characteristic of the asymptotic evolution of the turbulence.

To reduce the initial drop in K, Re_λ, and SK/ϵ, an alternative initialization method is introduced. The actual simulation of a stratified shear flow uses as initial fields the resulting fields of a simulation of unstratified unsheared isotropic turbulence. The initial value of the Reynolds number of the initialization simulation is chosen such that the final value matches the target initial Reynolds number of the actual simulation. The initialization simulation is advanced for about one eddy-turnover time and thus beyond the initial transient. During this time the skewness of $\partial u/\partial x$, which is a measure of the spectral transport, increases from zero to a final value $Sk = -0.46$. This value is in good agreement with other experimental and numerical results of $-0.5 < Sk < -0.4$ (Lesieur 1993). From the shape of the spectrum of these simulations the following alternative exponential spectrum was derived:

$$E(k) = E_0 k^2 \exp(-2k/k_0). \tag{3.3}$$

The results of simulations started from these initial conditions are also shown in

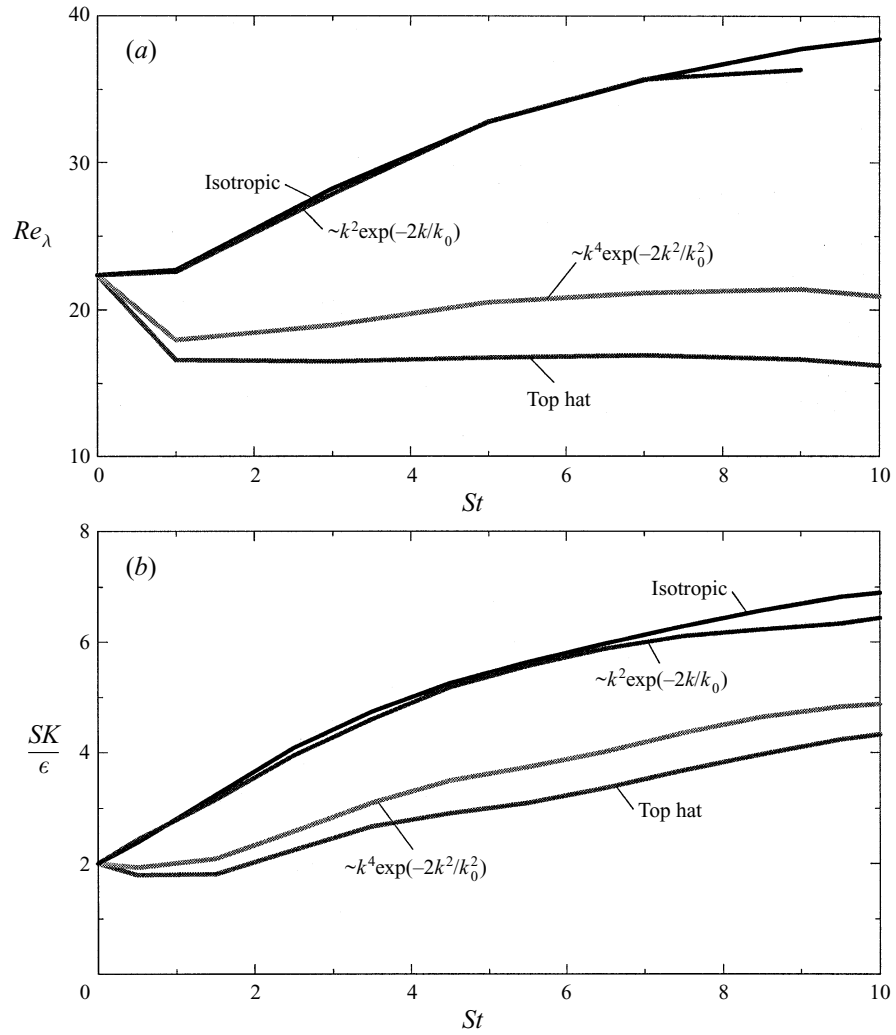

FIGURE 3. Evolution of (*a*) the Reynolds number Re_λ and (*b*) the shear number SK/ϵ for different initial spectra.

figures 2, 3(*a*) and 3(*b*). They result only in a small initial decay of the turbulent kinetic energy K, which has a physical explanation that will be discussed in §4. Neither Re_λ nor SK/ϵ show an initial drop. The simulations initialized with spectra (3.2) and (3.3) use a peak wavenumber $k_0 = 8$. The spectrum of the isotropic turbulence has a peak wavenumber $k_0 = 7$. The simulation initialized with the top-hat spectrum uses the wavenumbers $k_1 = 6$ and $k_2 = 12$.

During the initial transient, the energy spectrum defined by the initial conditions evolves into a spectrum characteristic for shear flow. Figure 4(*a*) shows the evolution of the spectrum for the simulation started from isotropic initial conditions. In the initial phase of the simulation ($0 < St < 5$), the low-wavenumber portion gains energy, and the high-wavenumber portion loses energy, but the general shape of the spectrum changes only slightly. A very similar evolution, though not shown, was observed for the spectrum of the simulation initialized with spectrum (3.3). Figure 4(*b*) shows the evolution of the spectrum for the simulation initialized with

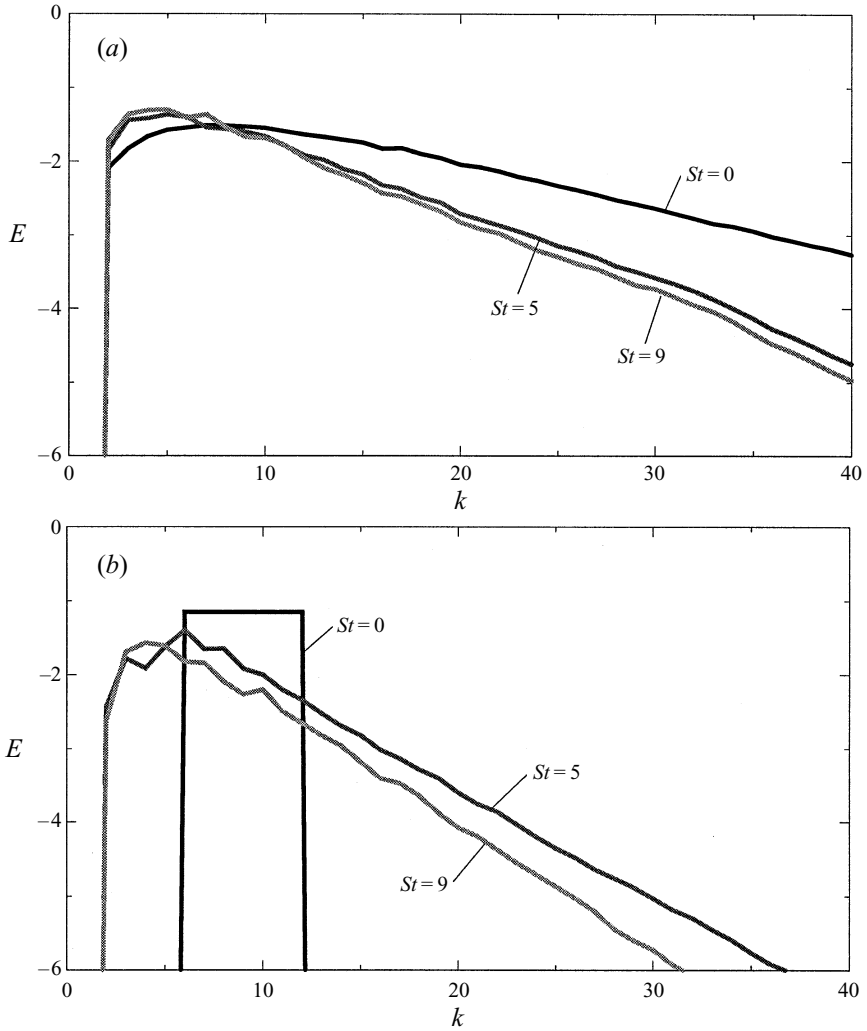

FIGURE 4. Evolution of the energy spectrum (*a*) for isotropic initial conditions and (*b*) for random initial conditions with a top-hat spectrum.

the top-hat spectrum. Comparison shows that the initial state does not contain a sufficient amount of energy at the lowest wavenumbers and in the high-wavenumber portion of the spectrum. During the initial transient, energy is redistributed into these wavenumber portions. This increases strongly the viscous dissipation ϵ, which in turn results in the large drop of SK/ϵ and Re_λ. This renders the initial values of these parameters uncharacteristic for the prediction of the asymptotic state of the flow. A similar evolution was observed for the spectrum of the simulation initialized with spectrum (3.2).

The initial condition of well-developed isotropic turbulence from a previous direct numerical simulation was chosen, because it represents a solution of the equations of motion for unstratified unsheared flow, and it allows an effective parameterization based on initial values. Isotropic initial conditions also compare better with the initial conditions found in experiments, where nearly isotropic conditions develop behind the turbulence-generating grid before the effects of shear and stratification become

	Ri	Re_λ	SK/ϵ	Grid size
Ri series	0.0	44.72	2.0	128^3
	0.08	44.72	2.0	128^3
	0.12	44.72	2.0	128^3
	0.16	44.72	2.0	128^3
	0.20	44.72	2.0	128^3
Re_λ series	0.08	11.18	2.0	96^3
	0.08	22.36	2.0	96^3
	0.08	33.54	2.0	128^3
	0.08	44.72	2.0	128^3
	0.08	67.08	2.0	144^3
	0.08	89.44	2.0	144^3
SK/ϵ series	0.06	22.36	0.2	96^3
	0.06	22.36	0.5	96^3
	0.06	22.36	1.0	96^3
	0.06	22.36	2.0	96^3
	0.06	22.36	4.0	96^3
	0.06	22.36	6.0	128^3
	0.06	22.36	8.0	128^3
	0.06	22.36	10.0	128^3

TABLE 1. Overview of the simulations described in this section. The simulations are initialized with well-developed isotropic turbulence fields with no density fluctuations. The molecular Prandtl number $Pr = 0.72$ is fixed.

important. All the shear flow simulations presented in this paper are based on the initialization method using well-developed isotropic turbulence fields obtained from a separate isotropic turbulence simulation initialized with spectrum (3.3).

4. Evolution of the kinetic energy

This section presents the results of a series of simulations, in which the Richardson number Ri, the initial value of the Reynolds number Re_λ, and the initial value of the shear number SK/ϵ are varied independently. Each section describes the influence of one parameter on the turbulent kinetic energy evolution and gives a physical explanation for that influence.

Table 1 gives an overview of the simulations described in this section. All simulations are initialized with velocity fields taken from simulations of unstratified unsheared decaying isotropic turbulence with no density fluctuations. The molecular Prandtl number $Pr = 0.72$ is fixed.

4.1. *Richardson number dependence*

All simulations show qualitatively the same dependence on Ri. Therefore one set of simulations with the initial values $Re_\lambda = 44.72$ and $SK/\epsilon = 2.0$ is discussed here.

Figure 5(*a*) shows the evolution of the turbulent kinetic energy K as a function of the non-dimensional time St with Ri as the variable parameter. After an initial decay K grows for small Richardson numbers and decays for high Richardson numbers. This makes it possible to define a critical Richardson number Ri_{cr} for the case of

constant K:

$$\frac{\mathrm{d}}{\mathrm{d}t}K \begin{cases} > 0 & \text{for } Ri < Ri_{cr} \\ = 0 & \text{for } Ri = Ri_{cr} \\ < 0 & \text{for } Ri > Ri_{cr}. \end{cases} \tag{4.1}$$

The initial decay in all cases is due to the isotropic initial conditions that cause the production term $P = -S\overline{u_1 u_3}$ to be initially zero. During the initial phase the production term grows. The initial decay has been observed in other numerical simulations (Gerz *et al.* 1989 and Holt *et al.* 1992) and experimental investigations (Rohr *et al.* 1988 and Piccirillo & Van Atta 1997).

In the case of homogeneous turbulent unstratified shear flow, experiments (Tavoularis & Karnik 1989) and direct numerical simulations (Rogers *et al.* 1986) support eventual exponential growth of the turbulent kinetic energy K. Rohr *et al.* (1988) have suggested that the evolution of K in the stratified case may also be exponential. An expression for the non-dimensional growth rate γ is obtained by rewriting the transport equation for the turbulent kinetic energy (2.9):

$$\gamma = \frac{1}{SK}\frac{\mathrm{d}K}{\mathrm{d}t} = -2b_{13}\left(1 - \frac{\epsilon}{P} - \frac{B}{P}\right). \tag{4.2}$$

Here b_{13} is the 1–3 component of the shear stress anisotropy tensor $b_{ij} = \overline{u_i u_j}/\overline{u_k u_k} - \delta_{ij}/3$. Under the assumption that each term on the right-hand side of equation (4.2) evolves to an asymptotically constant value for large non-dimensional time St, the equation can be integrated to obtain

$$K = K_0 \exp(\gamma St). \tag{4.3}$$

The exponential approximation is also shown with dashed lines in figure 5(a). The constant of integration is used to fit the graphs. The agreement shows that exponential growth or decay of the turbulent kinetic energy K is a good approximation. The exponential decay of K for the case $Ri > Ri_{cr}$ is different from the power law decay observed in unsheared decaying initially isotropic turbulence behind a grid. Figure 5(b) shows the evolution of the growth rate γ. Note that a positive value of γ is associated with growth and a negative value with decay of the turbulent kinetic energy K. The asymptotic value of the growth rate γ is positive for small Ri and negative for large Ri. The evolution of the anisotropy b_{13} is shown in figure 6. The magnitude of b_{13} decreases with increasing Ri. Therefore the effect of stratification reduces the anisotropy of the flow introduced by the effect of shear. Figure 7(a) shows the evolution of ϵ/P for various Ri. The asymptotic value of ϵ/P increases with increasing Ri. The evolution of B/P is presented in figure 7(b). The asymptotic value of the ratio B/P increases with increasing Ri.

The value of the critical Richardson number for this set of simulations is about $Ri_{cr} = 0.167$. (The method used to obtain the value of Ri_{cr} is described in §6.) While the other sets show qualitatively the same Richardson number dependence, the value of Ri_{cr} varies when the initial values of parameters such as Re_λ and the SK/ϵ are changed. The previous numerical simulations (Gerz *et al.* 1989 and Holt *et al.* 1992) and previous experimental investigations (Rohr *et al.* 1988 and Piccirillo & Van Atta 1997) found the same qualitative influence of the Richardson number, but the reported values of Ri_{cr} and the dependence of Ri_{cr} on other parameters in these investigations show significant differences. This will be addressed in §6.

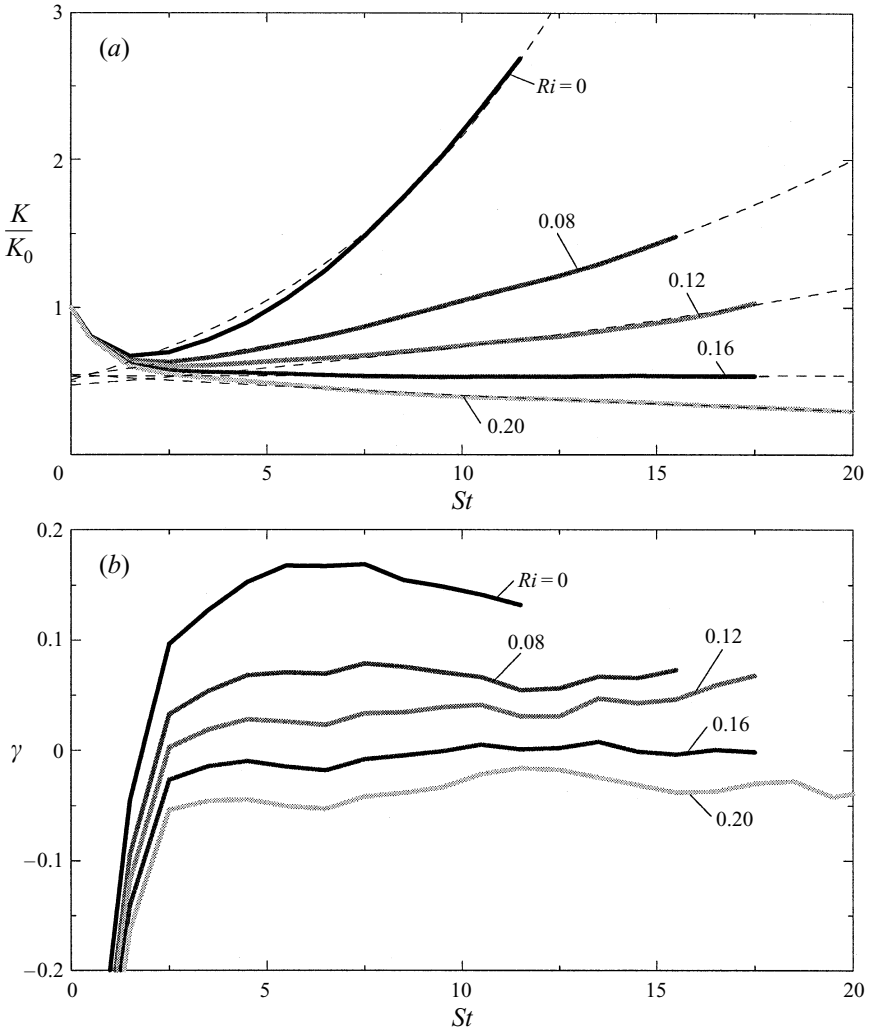

FIGURE 5. Evolution of (*a*) K and (*b*) γ as a function of Ri. The initial values of the $Re_\lambda = 44.72$ and $SK/\epsilon = 2.0$ are fixed. The dashed line shows the exponential approximation of equation (4.3).

To investigate the influence of shear and buoyancy, the turbulent kinetic energy equation is rewritten in a non-dimensional form:

$$\frac{1}{\epsilon}\frac{\mathrm{d}K}{\mathrm{d}t} = \frac{P}{\epsilon} - \frac{B}{\epsilon} - 1. \tag{4.4}$$

Figures 8(*a*) and 8(*b*) show the evolution of B/ϵ and P/ϵ, respectively. As expected B/ϵ grows with the Richardson number. But this increase is too small to account for the change in the evolution of K. On the other hand P/ϵ decreases strongly with increasing Richardson number. Therefore the primary effect of buoyancy is not a direct sink for K through the buoyancy flux but is the indirect reduction of the shear-induced production of K. This result is in agreement with the previous investigations by Holt *et al.* (1992) and Rohr *et al.* (1988).

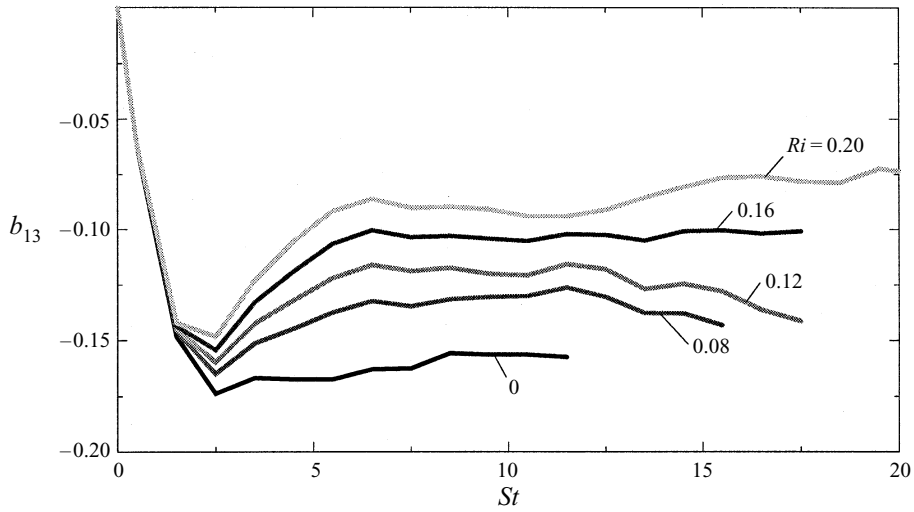

FIGURE 6. Evolution of b_{13} as a function of Ri. The initial values of $Re_\lambda = 44.72$ and $SK/\epsilon = 2.0$ are fixed.

4.2. *Reynolds number dependence*

In this subsection the results from simulations with a fixed Richardson number $Ri = 0.08$ and a fixed initial value of the shear number $SK/\epsilon = 2.0$ are presented. The initial value of the Taylor microscale Reynolds number Re_λ is varied within the range accessible in this investigation to study its influence on the turbulence evolution.

Figure 9(*a*) shows the evolution of the turbulent kinetic energy K. Initially K decays due to the isotropic initial conditions. This initial decay increases with increasing Re_λ. After this initial phase K continues to decay for small Re_λ but starts to grow for larger Re_λ.

The evolution of the exponential growth rate γ is shown in figure 9(*b*). For the low-Reynolds-number simulation with $Re_\lambda = 11.18$, the growth rate γ is negative, and the turbulent kinetic energy K decays. For a finite range of moderate Reynolds numbers with $Re_\lambda \leqslant 44.72$, the growth rate γ increases with increasing Re_λ, becomes positive, and reaches a maximum. For even higher Reynolds numbers $Re_\lambda > 44.72$, the growth rate γ decreases slightly with increasing Re_λ and appears to become relatively insensitive to Re_λ.

A necessary requirement for the Reynolds number independence of the growth rate γ is that the turbulent dissipation rate varies according to the high-Reynolds-number scaling $\epsilon = Au^3/l$ where A is a constant of order 1. After examining experimental data on grid turbulence, Sreenivasan (1984) determined that $A = \epsilon l/u^3$ decreases with increasing Reynolds number and asymptotically reaches the value $A = 1.0$ for $u\lambda/\nu > 50$ or $Re_\lambda = q\lambda/\nu > 87$. Recently, Lohse (1994), in an analytical work that starts with a differential equation for the velocity structure function derived by Effinger & Grossmann (1987), shows that the coefficient A becomes constant for values of Re_λ greater than approximately 50. In the present work, the Reynolds number at the end of the simulations is in the range $40 < Re_\lambda < 110$. Thus, our observation of the turbulence growth rate becoming approximately independent at the higher Reynolds numbers in this range is consistent with the results of Sreenivasan (1984) and Lohse (1994).

The evolution of the anisotropy b_{13} is presented in figure 10 for various initial

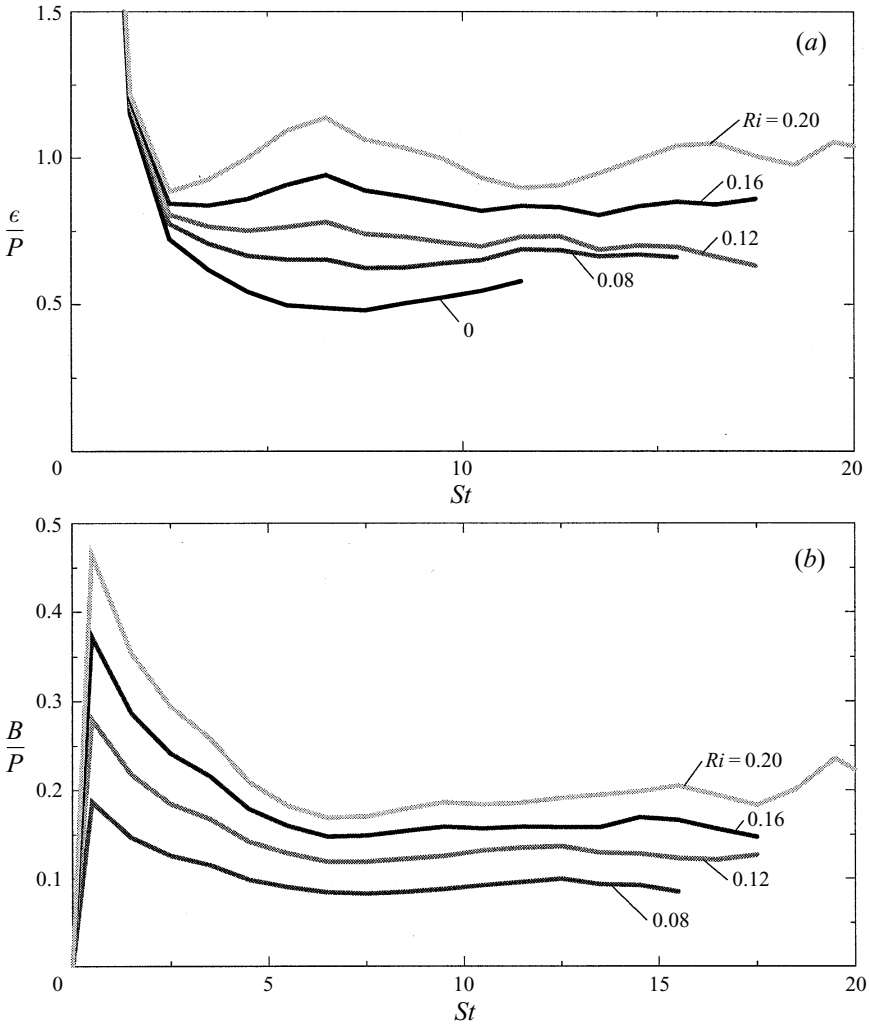

FIGURE 7. Evolution of (*a*) ϵ/P and (*b*) B/P as a function of *Ri*. The initial values of $Re_\lambda = 44.72$ and $SK/\epsilon = 2.0$ are fixed.

values of Re_λ. The asymptotic value of b_{13} decreases with increasing Re_λ and finally reaches a constant value independent of Re_λ. Figure 11(*a*) shows the evolution of ϵ/P for various Re_λ. The asymptotic value of ϵ/P decreases with increasing Re_λ for $Re_\lambda \leqslant 44.72$. For $Re_\lambda > 44.72$ the ratio ϵ/P increases with increasing Re_λ but finally becomes independent of Re_λ. From equation (4.2) it is clear that the minimum of ϵ/P at $Re_\lambda = 44.72$ causes the maximum of the growth rate γ at this Reynolds number. The evolution of B/P is shown in figure 11(*b*). The asymptotic value of the ratio B/P becomes approximately independent of the Reynolds number for $Re_\lambda \geqslant 44.72$.

4.3. *Shear number dependence*

In this subsection the dependence of the turbulence evolution on the initial value of the shear number SK/ϵ is addressed. The Richardson number $Ri = 0.06$ and the initial value of the Reynolds number $Re_\lambda = 22.36$ are fixed.

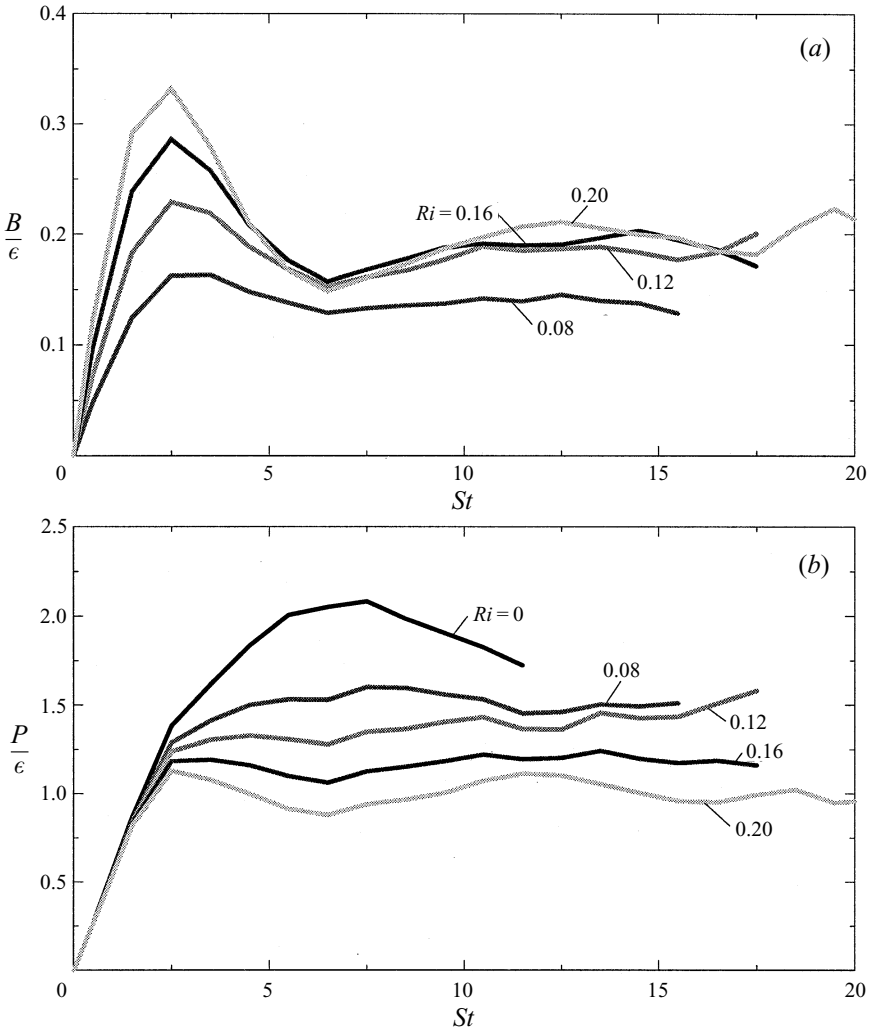

FIGURE 8. Evolution of (*a*) B/ϵ and (*b*) P/ϵ as a function of *Ri*. The initial values of $Re_\lambda = 44.72$ and $SK/\epsilon = 2.0$ are fixed.

In figure 12(*a*) the evolution of the turbulent kinetic energy K is presented as a function of SK/ϵ. Initially K decays due to the isotropic initial conditions. This decay is stronger for the simulations with a smaller SK/ϵ, because for these simulations the turbulence time scale K/ϵ is small compared to the shear time scale $1/S$. Therefore the turbulence has more time to decay before the turbulence production due to shear becomes significant. The growth rate γ of the turbulent kinetic energy is shown in figure 12(*b*).

The further evolution of the turbulent kinetic energy K can be divided into three regimes. First, for the low-shear-number simulation with $SK/\epsilon = 0.2$, the growth rate γ is negative, and K continues to decay. For this case the turbulence production due to shear P is always smaller than the turbulence destruction due to buoyancy effects B and viscous dissipation ϵ, that is $P < B + \epsilon$. Second, for a finite regime of moderate shear numbers $0.5 \leqslant SK/\epsilon \leqslant 6.0$, the growth rate γ is positive, and K grows. The turbulence production is larger than the turbulence destruction, that is $P > B + \epsilon$. Third,

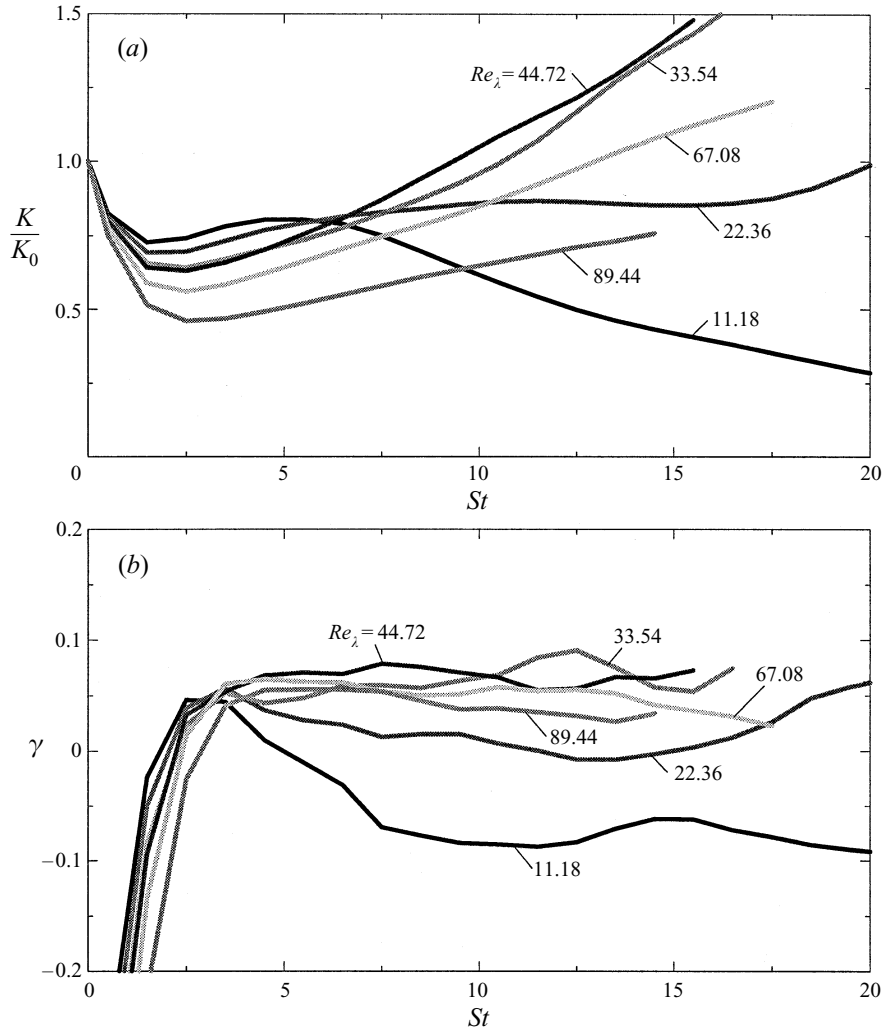

FIGURE 9. Evolution of (*a*) K and (*b*) γ as a function of the initial value of the Reynolds number. $Ri = 0.08$ and the initial value of $SK/\epsilon = 2.0$ are fixed.

for large shear numbers $SK/\epsilon > 6.0$, the growth rate γ is negative, and K decays again. This decay is due to a strongly reduced turbulence production as will be shown below.

Although the decay of the turbulent kinetic energy K for high shear numbers seems counterintuitive, there is an explanation for this effect. Consider the unstratified case first. For high SK/ϵ, linear effects dominate the turbulence evolution, and rapid distortion theory (RDT) applies at least for short times. It is known, see for example Rogallo (1981) and Rogers (1991), that viscous RDT predicts eventual decay of the velocity fluctuations after an initial period of algebraic growth. Direct numerical simulations of rapidly sheared turbulence with initial $SK/\epsilon = 13$ by Lee, Kim & Moin (1990) show that the magnitude of shear stress anisotropy b_{13} and the growth rate γ are substantially smaller than corresponding values for the moderately sheared case. Their simulations extended up to $St = 12$ which corresponds to approximately one eddy turnover time. Whether the stabilizing effect of high shear numbers persists at large non-dimensional time St in the unstratified case is probably still an open question.

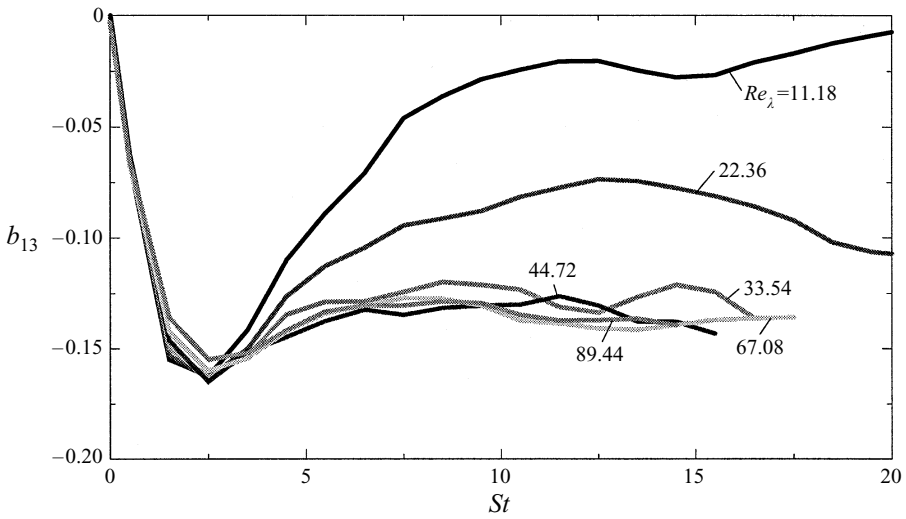

FIGURE 10. Evolution of b_{13} as a function of the initial value of the Reynolds number. $Ri = 0.08$ and the initial value of $SK/\epsilon = 2.0$ are fixed.

Now consider the stably stratified case. For the initial shear number SK/ϵ to have an influence on the evolution of the turbulent kinetic energy K, it is enough that the stabilizing rapid distortion effect persists for a time that is long enough for stratification effects to become important. For $Ri = 0.06$, the interval $St = 12$ in the DNS of Lee *et al.* (1990) corresponds to $Nt = 3$ which is sufficiently long. Therefore, the strongly sheared, stratified cases show substantially reduced values of γ in figure 12(*b*). The temporal oscillations in the evolution of γ are associated with the Brunt–Väisälä period, N. The $SK/\epsilon = 8.0$ simulation which shows eventual decay of turbulence was continued to a large value of $St = 30$, equivalent to approximately 7 Brunt-Väisälä periods and 3.75 eddy turnover times. These characteristic times are long enough to surmise that large shear numbers have a significant effect on the asymptotic fate of the turbulence evolution in a stratified shear flow.

The shear number range for which the turbulence asymptotically grows decreases with increasing Richardson number. For sufficiently large Richardson numbers the range of growth disappears, and the turbulent kinetic energy K always decays.

In figure 13 the evolution of the anisotropy b_{13} is shown. The asymptotic value of the magnitude of b_{13} decreases with increasing SK/ϵ. Figure 14(*a*) shows the evolution of ϵ/P. The asymptotic value of ϵ/P decreases with SK/ϵ for $SK/\epsilon \leqslant 4.0$, reaches a minimum, and finally increases with SK/ϵ for $SK/\epsilon > 4.0$. The minimum of ϵ/P at $SK/\epsilon = 4.0$ corresponds to a maximum of the growth rate γ at this shear number. The evolution of B/P is presented in figure 14(*b*). The asymptotic value of B/P is nearly independent of SK/ϵ.

The stabilizing effect of large initial values of SK/ϵ is associated with, first, a decrease of the asymptotic values of b_{13} as shown in figure 13 and, second, an increase of ϵ/P. The first effect is on the large-scale, energy-containing eddies that appears in rapid distortion analysis too. The second effect on $\epsilon/P = 1/(SK/\epsilon) * 1/(-2b_{13})$ is primarily due to the decrease of the asymptotic value of b_{13}. Although the final values of SK/ϵ are larger for larger initial values of SK/ϵ, the net effect is an increase of ϵ/P.

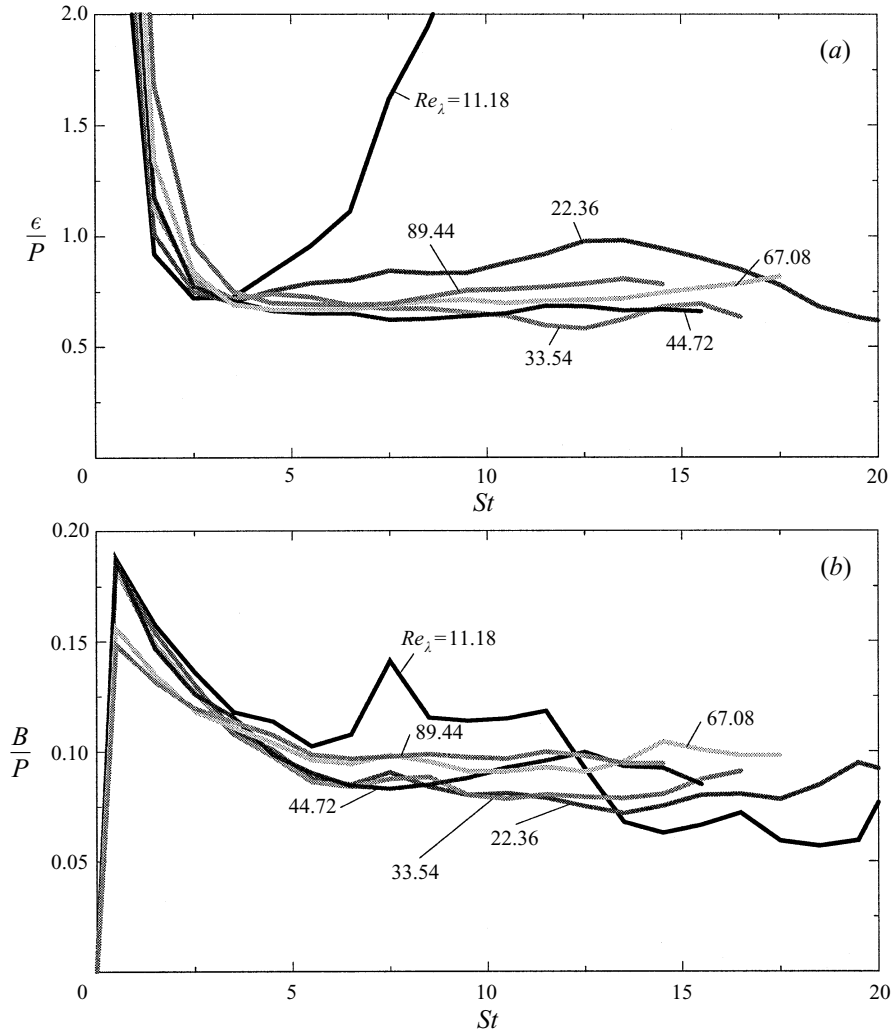

FIGURE 11. Evolution of (*a*) ϵ/P and (*b*) B/P as a function of the initial value of the Reynolds number. $Ri = 0.08$ and the initial value of $SK/\epsilon = 2.0$ are fixed.

5. Dependence of the asymptotic growth rate

In this section the dependence of the asymptotic values of the exponential growth rate γ on Ri and the initial values of Re_λ and SK/ϵ is summarized. The asymptotic values of the growth rate γ are computed as the average of the right-hand side of equation (4.2) for non-dimensional times $St > 8$.

Figure 15 shows the dependence of γ on Ri. The initial values of the Reynolds number $Re_\lambda = 44.72$ and the shear number $SK/\epsilon = 2.0$ are fixed. The growth rate γ decreases approximately linearly with increasing Ri.

The variation of γ with the initial value of Re_λ is presented in figure 16(*a*). The Richardson number $Ri = 0.08$ and the initial value of the shear number $SK/\epsilon = 2.0$ are fixed. For low Reynolds numbers, γ increases with increasing Re_λ. The growth rate γ reaches a maximum and decreases slightly. For high Reynolds numbers, γ tends to become independent of Re_λ.

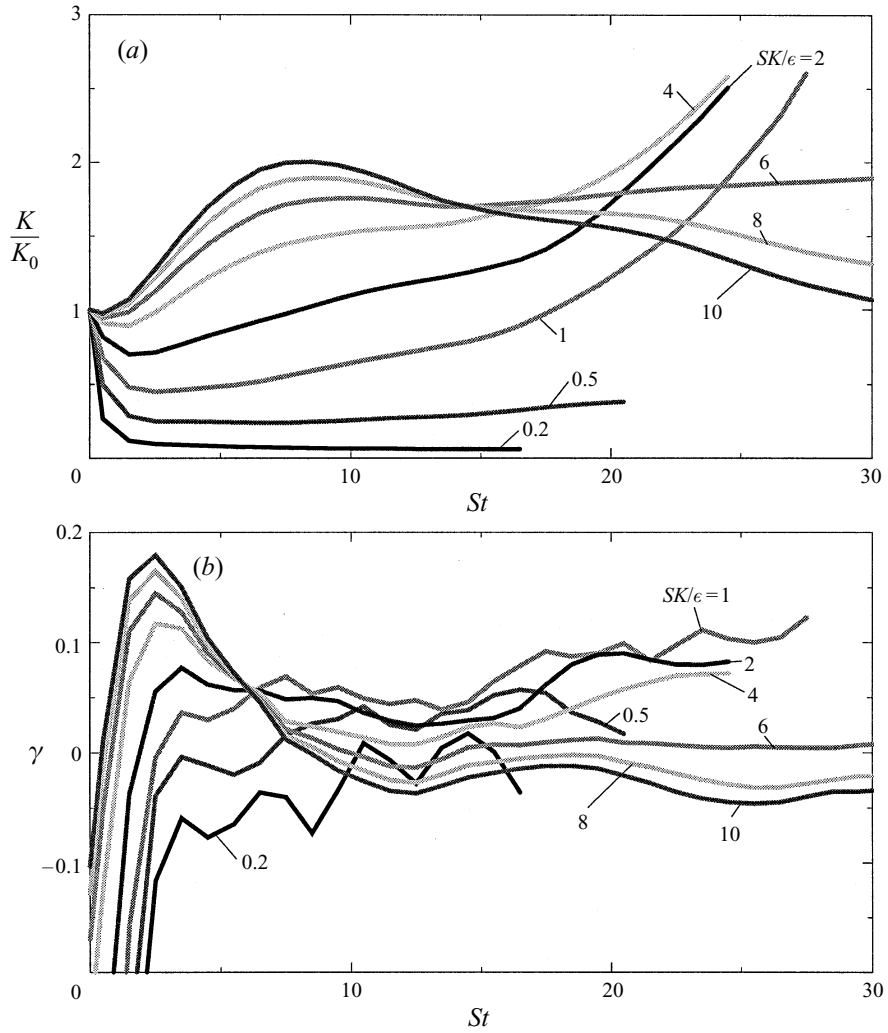

FIGURE 12. Evolution of (*a*) K and (*b*) γ as a function of the initial value of SK/ϵ. $Ri = 0.06$ and the initial value of $Re_\lambda = 22.36$ are fixed.

The dependence of γ on the initial value of SK/ϵ is shown in figure 16(*b*). The Richardson number $Ri = 0.06$ and the initial value of the Reynolds number $Re_\lambda = 22.36$ are kept constant. For low shear numbers, the growth rate γ increases with increasing SK/ϵ. The growth rate γ reaches a maximum and decreases with a further increase of SK/ϵ. Note that only a variation of SK/ϵ can lead to two critical cases with $\gamma = 0$.

The evolution of Re_λ for the series of simulations with different initial values of Re_λ is shown in figure 17(*a*). The Richardson number $Ri = 0.08$ and the initial value of the shear number $SK/\epsilon = 2.0$ are fixed. A parameterization of the exponential growth rate in terms of the initial value of Re_λ is meaningful, because the curves of the Reynolds number evolution do not intersect. In addition, the shape of the growth rate dependence on the Reynolds number, as shown in figure 16(*a*), does not change substantially with time.

Figure 17(*b*) shows the evolution of SK/ϵ for the series of simulations with different

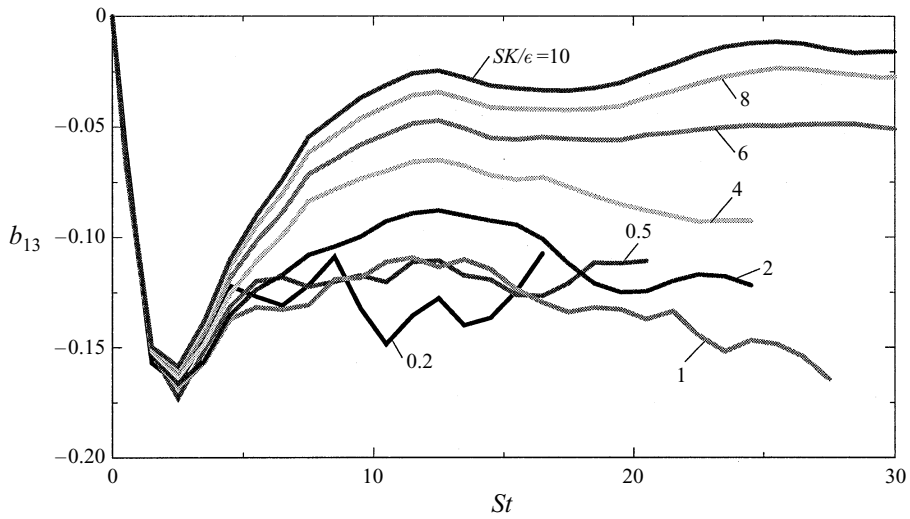

FIGURE 13. Evolution of b_{13} as a function of the initial value of SK/ϵ. $Ri = 0.06$ and the initial value of $Re_\lambda = 22.36$ are fixed.

initial values of SK/ϵ. The Richardson number $Ri = 0.06$ and the initial value of the Reynolds number $Re_\lambda = 22.36$ are fixed. The variation of γ can be presented in terms of the initial value of the shear number SK/ϵ, because the curves of the shear number evolution do not intersect. Also, the shape of the growth rate dependence on the shear number, as shown in figure 16(*b*), does not change substantially in time.

6. The critical Richardson number

The critical Richardson number Ri_{cr} is defined as the value of Ri for which the turbulent kinetic energy K stays constant in time. In §2.3 it was shown that the evolution of the turbulent kinetic energy K depends on Ri and the initial values of Re_λ and SK/ϵ. Therefore Ri_{cr} is a function of the initial values of Re_λ and SK/ϵ.

For the critical case, the turbulent kinetic energy equation (2.9) simplifies to

$$\frac{1}{\epsilon}\frac{\mathrm{d}K}{\mathrm{d}t} = \frac{P}{\epsilon} - \frac{B}{\epsilon} - 1 = 0 \tag{6.1}$$

or

$$\frac{B}{\epsilon} = \frac{P}{\epsilon} - 1. \tag{6.2}$$

The low-Reynolds-number scaling equations (2.21) and (2.22) for P/ϵ and B/ϵ lead to

$$Ri_{cr} = \frac{1}{\alpha}\frac{\lambda}{5l} Re_\lambda \frac{1}{SK/\epsilon}\left(\beta - \frac{1}{SK/\epsilon}\right). \tag{6.3}$$

The high-Reynolds-number scaling equations (2.24) and (2.25) for P/ϵ and B/ϵ lead to

$$Ri_{cr} = \frac{1}{\alpha}\frac{1}{SK/\epsilon}\left(\beta - \frac{1}{SK/\epsilon}\right). \tag{6.4}$$

The coefficients are

$$\alpha = 4\frac{\overline{u_3\rho}}{u_3^{rms}\rho^{rms}}\frac{u_3^{rms}}{q}\frac{L_e}{l}, \tag{6.5}$$

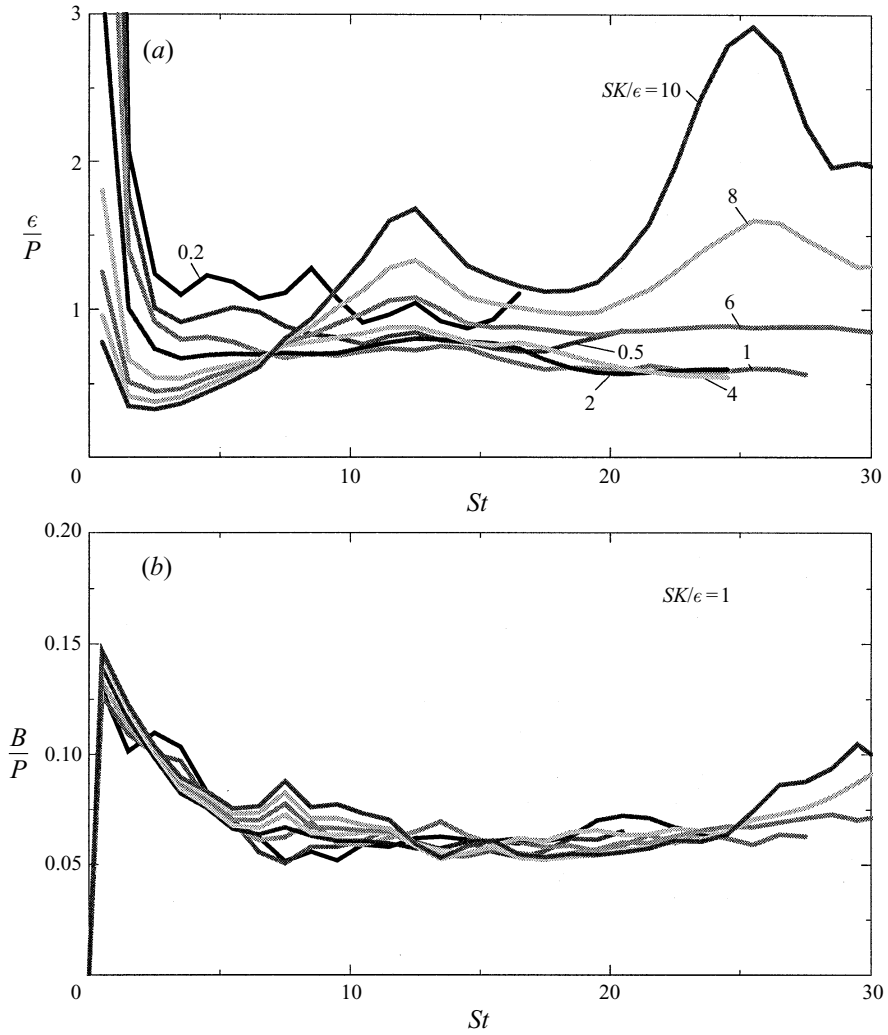

FIGURE 14. Evolution of (*a*) ϵ/P and (*b*) B/P as a function of the initial value of SK/ϵ. $Ri = 0.06$ and the initial value of $Re_\lambda = 22.36$ are fixed.

$$\beta = -2b_{13}. \tag{6.6}$$

This dependence of Ri_{cr} on Re_λ and SK/ϵ is exact for the instantaneous values of Re_λ, SK/ϵ, α, and β. In order to estimate the dependence of Ri_{cr} on the initial values of Re_λ and SK/ϵ we assume that, first, the coefficients α and β are constant and, second, the final values of Re_λ and SK/ϵ are monotone increasing functions of the initial values of Re_λ and SK/ϵ. The second assumption is a result of our direct numerical simulations, and the first assumption is a reasonable approximation to the turbulence state after an initial transient according to our direct numerical simulations.

Then, it can be expected from equation (6.3) that for low Reynolds numbers, Ri_{cr} grows linearly with increasing initial values of Re_λ and, from equation (6.4), that for high Re_λ the critical Richardson number Ri_{cr} becomes independent of Re_λ.

In addition, it can be expected that Ri_{cr} varies with the initial value of SK/ϵ as

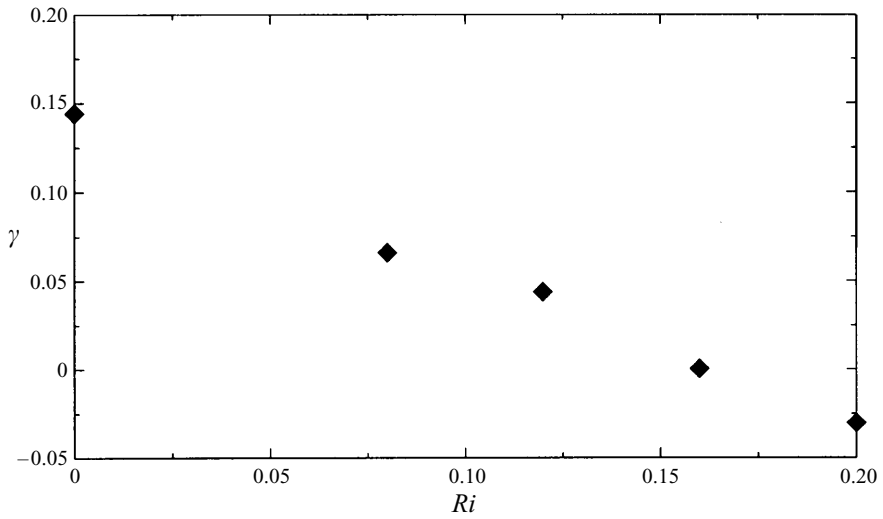

FIGURE 15. Variation of the asymptotic growth rate γ as a function of *Ri*. The initial values of $Re_\lambda = 44.72$ and $SK/\epsilon = 2.0$ are fixed.

given by equations (6.3) and (6.4). The shear number dependence in these equations shows that for small SK/ϵ, the critical Richardson number Ri_{cr} grows with increasing SK/ϵ, reaches a maximum, and finally decreases with a further increase of SK/ϵ. It is therefore possible to obtain the same value of Ri_{cr} for two different values of SK/ϵ.

Also note that the critical Richardson number can be negative for sufficiently small initial values of the Reynolds and shear numbers. In this case an unstable density stratification must be maintained to allow for a constant level of turbulence. The analysis presented here was inspired by an argument given in Townsend (1957).

Simulations were performed to find the dependence of the critical Richardson number Ri_{cr} on the initial values of the Reynolds number Re_λ and the shear number SK/ϵ numerically. In §5 it was shown that the exponential growth rate γ is approximately a linear function of the Richardson number *Ri*. Therefore the value of Ri_{cr} was determined by identifying two nearby Richardson numbers that cause growth and decay and using linear interpolation.

Figure 18(*a*) shows the variation of Ri_{cr} as a function of the initial value of Re_λ as determined by DNS. The initial value of SK/ϵ is kept constant in this series of simulations. The value of Ri_{cr} increases with the initial value of Re_λ. For large Re_λ, Ri_{cr} varies only slightly with Re_λ.

The dependence of Ri_{cr} on the initial value of SK/ϵ is shown in figure 18(*b*). In this series of simulations the initial value of Re_λ is kept constant. With increasing SK/ϵ, the critical Richardson number Ri_{cr} increases, reaches a maximum, and finally decreases. Therefore the same value of Ri_{cr} can be obtained at two different SK/ϵ.

Thus, the variation of the critical Richardson number Ri_{cr} as determined from DNS agrees qualitatively with the variation indicated by the scaling analysis of the transport equation for the turbulent kinetic energy.

The laboratory experiments of Piccirillo & Van Atta (1997) showed that when the mesh size (and thereby the microscale Reynolds number) of the grid was increased, Ri_{cr} decreased, in apparent contradiction to the finding of Holt *et al.* (1992) who found an increase in Ri_{cr} with increasing Reynolds number. After examination of the laboratory data, it was found that SK/ϵ decreases when the mesh size of the

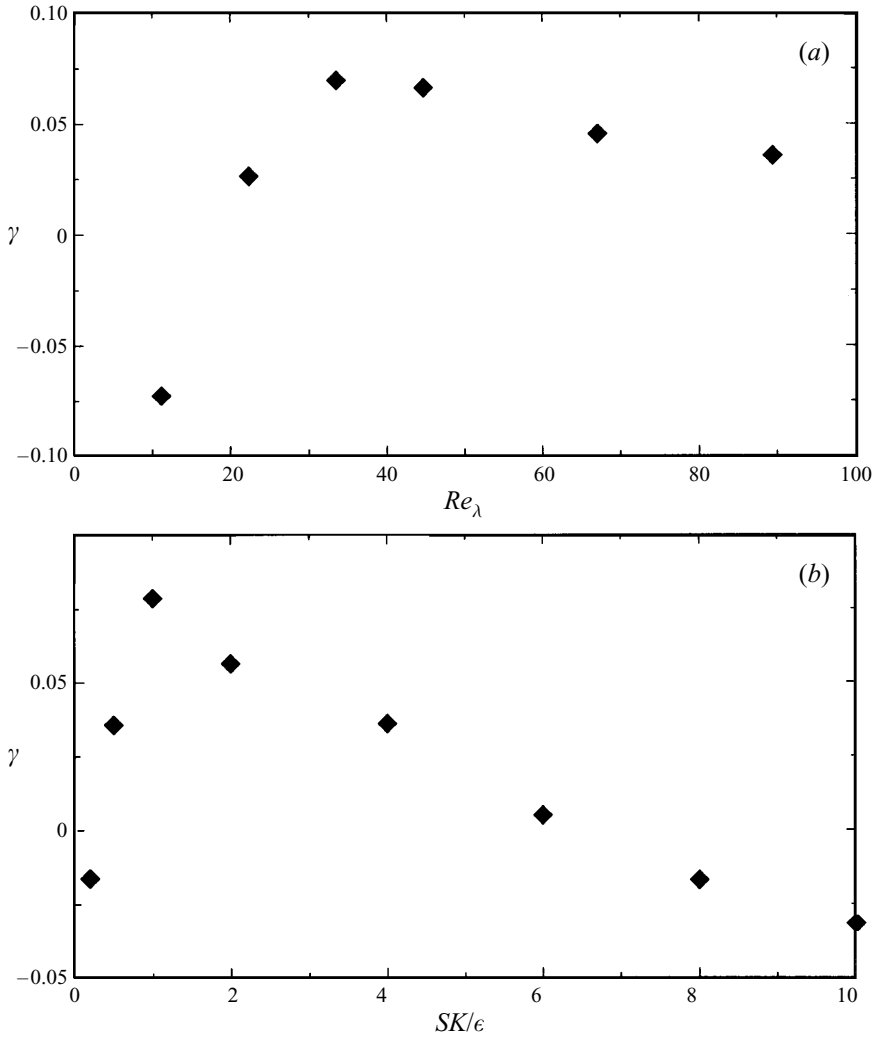

FIGURE 16. (*a*) Variation of the asymptotic growth rate γ as a function of Re_λ. $Ri = 0.08$ and the initial value of $SK/\epsilon = 2.0$ are fixed. (*b*) Variation of the asymptotic growth rate γ as a function of SK/ϵ. $Ri = 0.06$ and the initial value of $Re_\lambda = 22.36$ are fixed.

grid increases. The shear number values in the laboratory were below 0.5, placing them in the left-hand corner of the plot in figure 18(*b*) and thus in the range where Ri_{cr} decreases with decreasing SK/ϵ. Thus, the decrease in Ri_{cr} with increasing mesh size in the laboratory experiment may be a shear number effect and not a Reynolds number effect.

7. Conclusions

In this investigation, a spectral collocation method for the direct numerical simulation of homogeneous turbulence in a stratified shear flow was implemented and validated. In addition, the importance of carefully defined initial conditions for an effective parameterization of the turbulence evolution was addressed. A dimensional analysis was performed to derive the non-dimensional parameters governing the tem-

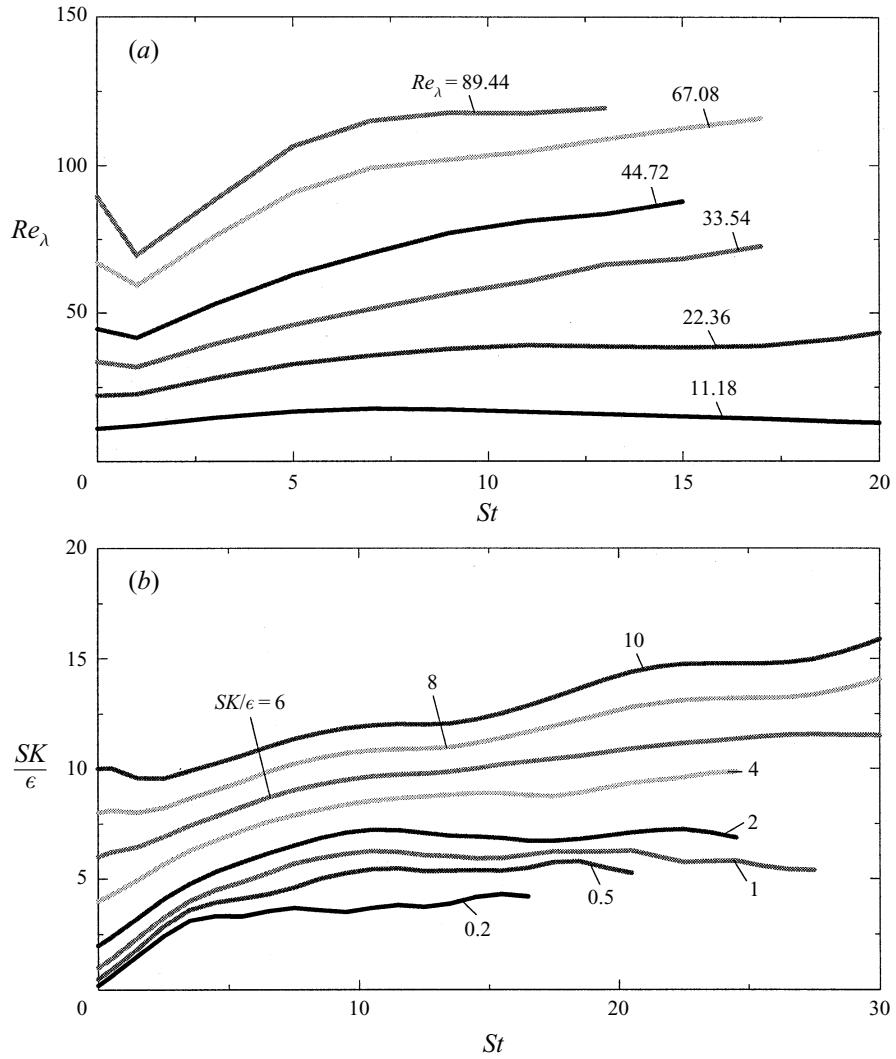

FIGURE 17. (*a*) Evolution of Re_λ for the series of simulations with initially different Reynolds numbers. $Ri = 0.08$ and the initial value of $SK/\epsilon = 2.0$ are fixed. (*b*) Evolution of SK/ϵ for the series of simulations with initially different shear numbers. $Ri = 0.06$ and the initial value of $Re_\lambda = 22.36$ are fixed.

poral development of the turbulence. These parameters are the Richardson number Ri, the Reynolds number Re_λ, and the shear number SK/ϵ. From the simulations, it was found that, for a given spectral shape of the initial fluctuations, the evolution of the turbulent kinetic energy K depends strongly on Ri and the initial values of Re_λ and SK/ϵ. Furthermore, it was shown that the evolution of K follows approximately an exponential law.

The variation of the asymptotic value of the exponential growth rate γ with Ri, the initial value of Re_λ, and the initial value of SK/ϵ is shown in figures 15, 16(*a*), and 16(*b*), respectively. The growth rate γ decreases approximately linearly with increasing Ri. The stabilizing influence of the Richardson number on the turbulent kinetic energy is not caused by the explicit sink associated with the buoyancy flux. It

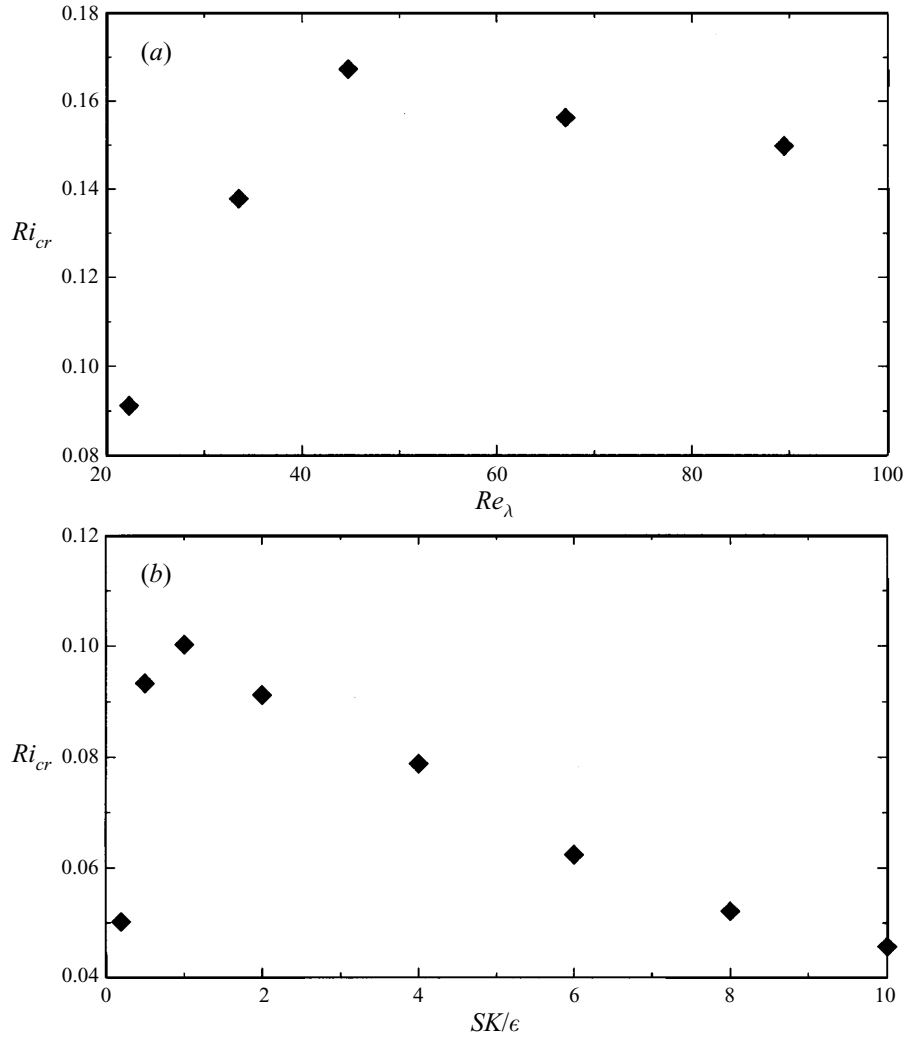

FIGURE 18. (*a*) Variation of Ri_{cr} as a function of the initial value of Re_λ. The initial value of $SK/\epsilon = 2.0$ is fixed. (*b*) Variation Ri_{cr} as a function of the initial value of SK/ϵ. The initial value of $Re_\lambda = 22.36$ is fixed.

is due to the decreasing value of the relative turbulence production P/ϵ as well as the decreasing magnitude of Reynolds shear stress anisotropy b_{13} with increasing Ri.

The growth rate γ increases with increasing initial values of Re_λ but finally tends to become independent for high Re_λ.

The dependence of γ on the initial value of SK/ϵ is non-monotone. The growth rate γ increases, reaches a maximum, and finally decreases with increasing SK/ϵ. The decrease of γ as a function of SK/ϵ for large shear numbers is consistent with linear viscous RDT results. Although RDT is strictly applicable for short times only, DNS shows that the qualitative effect of the shear number suggested by RDT persists for long times too. The stabilizing effect of increased shear number is associated mainly with a decreased Reynolds shear stress anisotropy b_{13} and also has a contribution from a reduced relative production P/ϵ. The shear number effect discussed here is based on simulations at an initial Reynolds number $Re_\lambda = 22.36$ (final values as large

as $Re_\lambda \simeq 50$) and a Richardson number $Ri = 0.06$. It is probable that the detailed influence of the shear number may vary with the initial value of the Reynolds number and the Richardson number and should be the subject of a future study.

The critical Richardson number Ri_{cr} is of interest, because for $Ri < Ri_{cr}$ the asymptotic fate of the turbulence is growth as opposed to decay for $Ri > Ri_{cr}$. The value of Ri_{cr} was found to depend on the initial values of Re_λ and SK/ϵ. The variation of Ri_{cr} with Re_λ and SK/ϵ is shown in figures 18(*a*) and 18(*b*), respectively. The variation of Ri_{cr} in the DNS is large, ranging from 0.04 at the lowest values of Reynolds and shear number to a high of 0.17. Thus in nonlinearly evolving uniform shear flow, the estimate of $Ri_{cr} = 0.25$ motivated by the linear result of Miles (1961) is not applicable. The simple scaling analysis of the turbulence transport equation in §6 also suggests that Ri_{cr} varies as a function of Reynolds and shear numbers. The critical Richardson number Ri_{cr} increases and finally tends to become independent with increasing Re_λ. This result is consistent with the results reported by Holt *et al.* (1992). The critical Richardson number Ri_{cr} increases, reaches a maximum, and finally decreases with increasing SK/ϵ. This shear number dependence of Ri_{cr} may explain the experimental results of Piccirillo & Van Atta (1997). In their study a decrease of Ri_{cr} with increasing grid size (and therefore increasing Re_λ by a moderate amount and decreasing SK/ϵ) was observed. Based on our numerical study, it appears that the increase of Re_λ does not cause a decrease of Ri_{cr}. However, the decrease of the already small SK/ϵ contributes to the decrease of Ri_{cr}. The dependence of Ri_{cr} on both Re_λ and SK/ϵ observed in the DNS agrees qualitatively with results obtained from a scaling analysis of the transport equation of the turbulent kinetic energy.

The authors acknowledge the support from the Office of Naval Research, Physical Oceanography Program, through the grant ONR N00014-94-1-0223. F. G. Jacobitz was partially supported by the Deutschen Akademischen Austauschdienst (DAAD-Doktorandenstipendium aus Mitteln des zweiten Hochschulsonderprogramms). Supercomputer time was provided by the San Diego Supercomputer Center (SDSC) and the US Army Corps of Engineers Waterways Experiment Station (WES).

Appendix. Validation

To ensure the reliability of the numerical method used in this study, a number of validation simulations were performed. First, the solutions were compared with results obtained by Holt *et al.* (1992). Second, the influence of the resolution of the computational domain was investigated. Third, the universality of the non-dimensional parameters introduced in §2.3 was established.

Comparison with Holt et al. (1992)

A simulation was performed that matches the initial radial spectrum and the initial values of the non-dimensional parameters of the simulation labelled HD by Holt *et al.* (1992). The evolution of the normalized Reynolds stress $R^*_{13} = \overline{u_1 u_3}/(u_1^{rms} u_3^{rms})$ and of the normalized vertical transport $R^*_{3\rho} = \overline{u_3 \rho}/(u_3^{rms} \rho^{rms})$ is shown in figures 19(*a*) and 19(*b*), respectively. The computed values agree within 5%. The small differences can be attributed to different methods used to advance the solutions in time and to different initial random fields.

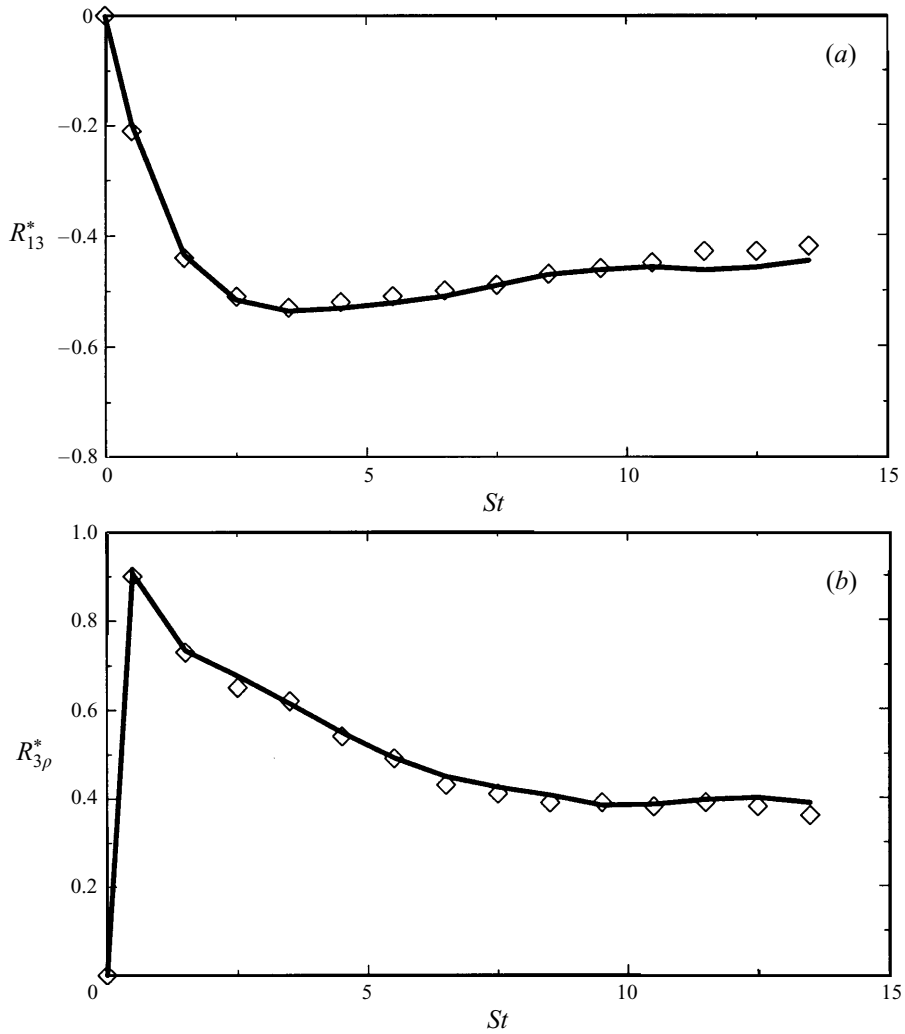

FIGURE 19. Evolution of (*a*) the normalized Reynolds stress $R^*_{13} = \overline{u_1 u_3}/(u_1^{rms} u_3^{rms})$ and (*b*) the normalized vertical transport $R^*_{3\rho} = \overline{u_3 \rho}/(u_3^{rms} \rho^{rms})$. The diamonds correspond to the values obtained by Holt *et al.* (1992).

Influence of spatial resolution

A simulation with the initial parameters $Ri = 0.08$, $Re_\lambda = 67.08$, and $SK/\epsilon = 2.0$ originally performed on a grid with 128^3 points was restarted at $St = 9.0$ on a grid with 144^3 points. The extrapolation necessary for this grid expansion was done in spectral space. Figure 20(*a*) shows the two-point correlations $R_{11}(x)$ at the non-dimensional time $St = 14$ of the two simulations performed on the 144^3 and 128^3 grids. Both cases show that $R_{11}(x)$ decays to zero for sufficiently large x. Therefore the resolution of the computational domain does not influence the evolution of the largest turbulence scales.

To ensure a sufficient resolution of the small turbulence scales the energy spectra $E(k)$ at the non-dimensional time $St = 14$ of the two simulations performed on the 144^3 and 128^3 grids are shown in figure 20(*b*). The spectra show an identical evolution

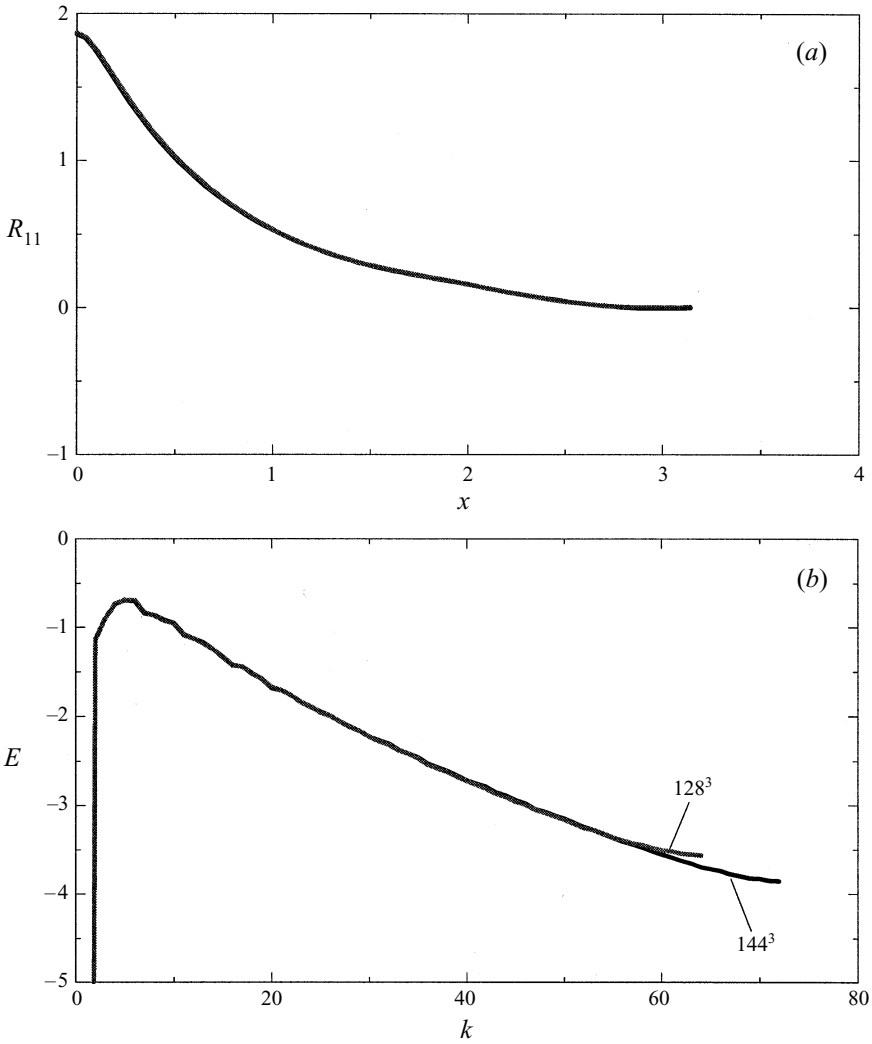

FIGURE 20. (*a*) Two-point correlations $R_{11}(x)$ and (*b*) energy spectra $E(k)$ of two simulations with the initial parameters $Ri = 0.08$, $Re_\lambda = 67.08$, and $SK/\epsilon = 2.0$ at the non-dimensional time $St = 14$. The original simulation performed on a grid with 128^3 points is compared with a simulation restarted at $St = 9.0$ on a grid with 144^3 points.

of the low-wavenumber portion and a sufficient resolution of the high-wavenumber portion of the spectra. Therefore the grid used has the high resolution required to obtain accurately the evolution of the turbulence.

Universality of the non-dimensional parameters

The universality of the non-dimensional parameters was checked by rescaling the initial conditions of a simulation with the initial parameters $Ri = 0.08$, $Re_\lambda = 67.08$, and $SK/\epsilon = 2.0$. The initial velocity fluctuations q are increased to a new value $q^* = 2q$. To keep the Reynolds number constant for a fixed initial spectrum, the kinematic viscosity has to be changed to a new value $\nu^* = 2\nu$. To keep the shear number SK/ϵ constant, the shear rate S has to be changed to a new value $S^* = 2S$. The ratio of the turbulent kinetic energies K^*/K obtained from the rescaled and

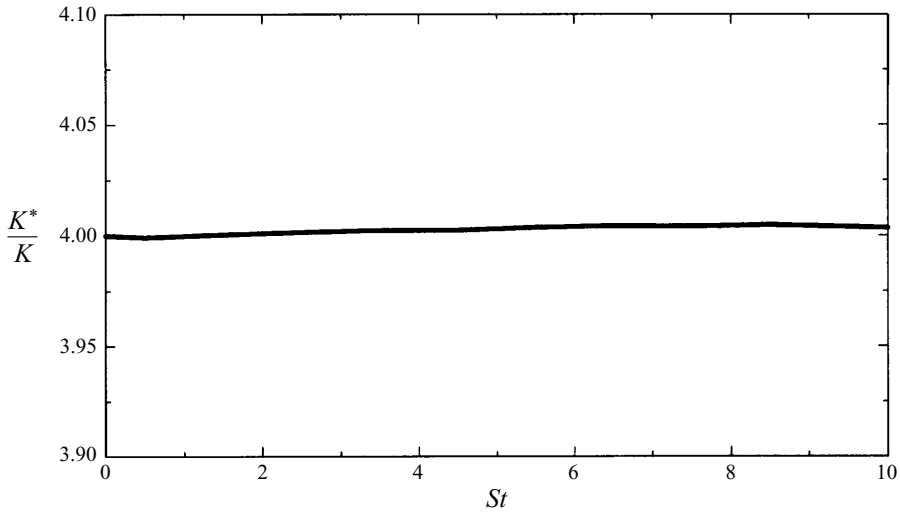

FIGURE 21. Evolution of the ratio of the turbulent kinetic energies K^*/K obtained from simulations using the rescaled and the original initial parameters, respectively.

original simulations is shown in figure 21. This ratio always remains very close to its initial value of 4.0 as it should. This shows the universality of the non-dimensional parameters derived in §2.3.

REFERENCES

BATCHELOR, G. K. 1953*a* *The Theory of Homogeneous Turbulence*. Cambridge University Press.

BATCHELOR, G. K. 1953*b* The conditions for dynamical similarity of the motions of a frictionless perfect gas atmosphere. *Q. J. R. Met. Soc.* **79**, 224–235.

EFFINGER, H. & GROSSMANN, S. 1987 Static structure function of turbulent flow from the Navier-Stokes equations. *Zeit. Phys.* B *Cond. Matter* **66**, 289–304.

GERZ, T., SCHUMANN, U. & ELGHOBASHI, S. E. 1989 Direct numerical simulation of stratified homogeneous turbulent shear flows. *J. Fluid Mech.* **200**, 563–594.

GOLDSTEIN, S. 1931 On the stability of superposed streams of fluids of different densities. *Proc. R. Soc. Lond.* A **132**, 524–547.

HOLT, S. E., KOSEFF, J. R. & FERZIGER, J. H. 1992 A numerical study of the evolution and structure of homogeneous stably stratified sheared turbulence. *J. Fluid Mech.* **237**, 499–539.

HOWARD, L. N. 1961 Note on a paper of John W. Miles. *J. Fluid Mech.* **10**, 509–512.

HUNT, J. C. R. 1978 Review of the theory of rapidly distorted turbulent flows and its applications. *Fluid Dyn. Trans.* **9**, 121–152.

KALTENBACH, H.-J., GERZ, T. & SCHUMANN, U. 1994 Large-eddy simulation of homogeneous turbulence and diffusion in stably stratified shear flow. *J. Fluid Mech.* **280**, 1–40.

LEE, M. J., KIM, J. & MOIN, P. 1990 Structure of turbulence at high shear rate. *J. Fluid Mech.* **216**, 561–583.

LESIEUR, M. 1993 *Turbulence in Fluids*. Kluwer.

LOHSE, D. 1994 Crossover from high to low Reynolds number turbulence. *Phys. Rev. Lett.* **73**, 3223–3226.

MILES, J. W. 1961 On the stability of heterogeneous shear flows. *J. Fluid Mech.* **10**, 496–508.

MILES, J. W. 1986 Richardson's criterion for the stability of stratified shear flow. *Phys. Fluids* **29**, 3470–3471.

PICCIRILLO, P. S. & VAN ATTA, C. W. 1997 The evolution of a uniformly sheared thermally stratified turbulent flow. *J. Fluid Mech.* **334**, 61–86.

PRANDTL, L. 1930 Einfluß stabilisierender Kräfte auf die Turbulenz. In *Vorträge aus dem Gebiete der Aerodynamik und verwandter Gebiete, Aachen 1929* (ed. A. Gilles, L. Hopf & Th. von Kármán). Springer.

RICHARDSON, L. F. 1920 The supply of energy from and to atmospheric eddies. *Proc. R. Soc.* A **97**, 354–373.

ROGALLO, R. S. 1981 Numerical experiments in homogeneous turbulence. *NASA TM* 81315.

ROGERS, M. M. 1991 The structure of a passive scalar field with a uniform mean gradient in rapidly sheared homogeneous turbulent flow. *Phys. Fluids* A **3**, 144–154.

ROGERS, M. M., MOIN, P. & REYNOLDS, W. C. 1986 The structure and modeling of the hydrodynamic and passive scalar fields in homogeneous turbulent shear flow. *Rep.* TF-25, Dept. Mech. Engng., Stanford University, California.

ROHR, J. J., ITSWEIRE, E. C., HELLAND, K. N. & VAN ATTA, C. W. 1988 Growth and decay of turbulence in a stably stratified shear flow. *J. Fluid Mech.* **195**, 77–111.

SARKAR, S. 1995 The stabilizing effect of compressibility in turbulent shear flow. *J. Fluid Mech.* **282**, 163–186.

SAVILL, A. M. 1987 Recent developments in rapid-distortion theory. *Ann. Rev. Fluid Mech.* **19**, 531–575.

SOUZA, F. A. DE, NGUYEN, V. D. & TAVOULARIS, S. 1995 The structure of highly sheared turbulence. *J. Fluid Mech.* **303**, 155–167.

SREENIVASAN, K. R. 1984 On the scaling of the turbulence energy dissipation rate. *Phys. Fluids* **27**, 1048–1051.

TAVOULARIS, S. & KARNIK, U. 1989 Further experiments on the evolution of turbulent stresses and scales in uniformly sheared turbulence. *J. Fluid Mech.* **204**, 457–478.

TAYLOR, G. I. 1931 Effect of variation in density on the stability of superposed streams of fluid. *Proc. R. Soc. Lond.* A **132**, 499–523.

TOWNSEND, A. A. 1957 Turbulent flow in a stably stratified atmosphere. *J. Fluid Mech.* **3**, 361–372.